NUMERICAL ANALYSIS OF A CIRCULATION CONTROL WING

A Thesis

presented to

the Faculty of California Polytechnic State University,

San Luis Obispo

In Partial Fulfillment

of the Requirements for the Degree

Master of Science in Aerospace Engineering

by

Luke Bodkin

December 2020

COMMITTEE MEMBERSHIP

TITLE:	Numerical Analysis of a Circulation Control Wing
AUTHOR:	Luke Bodkin
DATE SUBMITTED:	December 2020
COMMITTEE CHAIR:	Aaron Drake, Ph.D. Professor of Aerospace Engineering
COMMITTEE MEMBER:	Paulo Iscold, Ph.D. Associate Professor of Aerospace Engineering
COMMITTEE MEMBER:	David Marshall, Ph.D. Department Chair Aerospace Engineering
COMMITTEE MEMBER:	Russell Westphal, Ph.D. Professor of Mechanical Engineering

ABSTRACT

Numerical Analysis of a Circulation Control Wing

Luke Bodkin

The objective of this thesis was to develop an experimental method to research circulation control wings using numerical analysis. Specifically, it is of interest to perform 3D wind tunnel testing on a circulation control wing in the Cal Poly Low Speed Wind Tunnel (CPLSWT). A circulation control wing was designed and analyzed to determine the feasibility of this testing.

This study relied on computational fluid dynamics (CFD) simulations as a method to predict the flow conditions that would be seen in a wind tunnel test. A CFD simulation was created of a wing model in a wind tunnel domain. Due to high computational requirements, reliable 3D CFD results were not obtained. This led to utilizing 2D CFD models to make estimations about the flow conditions that would be encountered in an experimental environment. The 2D CFD model was validated with previous experimental data on circulation control wings and was shown to accurately capture the flow physics. These 2D CFD results were used to create a set of guidelines to help improve the effectiveness of a future wind tunnel test campaign and demonstrate where further design work needs to be done.

The key finding is that it is feasible to perform circulation control testing in the CPLSWT with limitations on the maximum momentum coefficient. Due to internal plenum pressures reaching 66 psi at $C_\mu = 0.35$, a limitation should be placed on experimental testing below the choked condition of at $C_\mu = 0.15$. This provides a more feasible operating range for the equipment available. The main performance parameter of the airfoil was met with $C_{L\,MAX} = 5.01$ at $C_\mu = 0.35$ which required 0.9 lb/s/m mass flow rate for the 2D model.

ACKNOWLEDGMENTS

TABLE OF CONTENTS

LIST OF TABLES

Table Page

LIST OF FIGURES

Figure Page

Chapter 1

INTRODUCTION

Circulation control in this paper is specifically referring to a pneumatic jet blown tangential to a Coanda surface to modify the flow field around a wing as seen in Figure 1. Circulation control wings have been in development since the early 1960's.[4] There have been investigations into different applications – from rotor blades to tractor trailers.[4] However, this technology has not seen any adoption in the aerospace industry as of yet. There has been more recent interest by NASA in this technology beginning in the early 2000's.[7] This eventually led to a collaboration project between Cal Poly and NASA that culminated with wind tunnel testing of the AMELIA model in the NASA AMES National Full Scale Aerodynamics Complex (NFAC). [12]

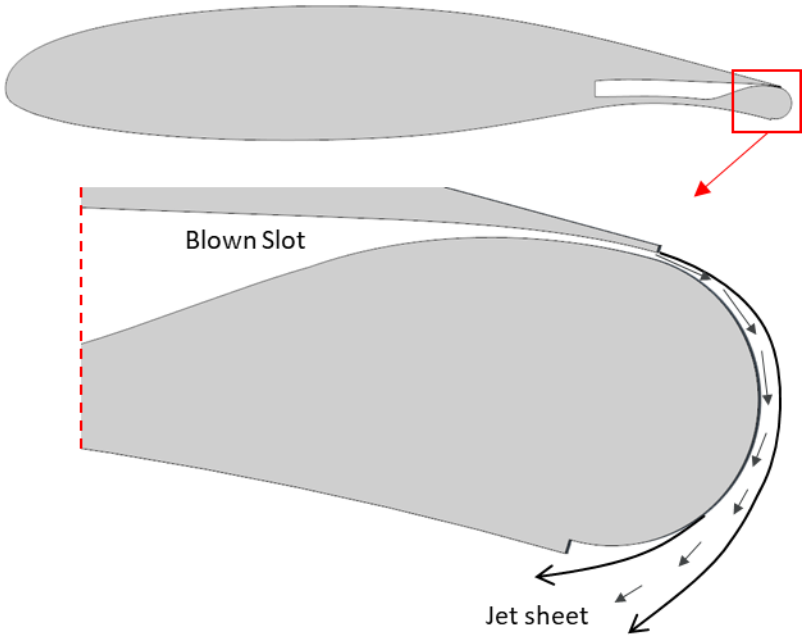

Figure 1. A typical circulation control airfoil with a circular trailing edge shape demonstrating the streamline turning of the jet sheet around the Coanda surface.

Circulation control has shown promise for many different sizes of aircraft. However, this technology has issues being applied in cruise for high speed aircraft due the requirement of the jet velocity being significantly higher than the freestream velocity. This leads to complexities with sustained supersonic flow at the jet exit. Personal aerial vehicle (PAV) and unmanned aerial vehicle (UAV) size range of air vehicles appear to be better candidates for this technology to be

applied throughout the flight regime. [8] It should be noted that the mass flow requirements for circulation control are typically assumed to come from either bleed air from the engine or an auxiliary power unit. These air sources will have varying related efficiencies, however reducing mass flow rate is a key performance metric for circulation control.

Previous numerical analysis and experimental investigation have been insufficient to provide the confidence necessary to apply this to a production air vehicle. It would be valuable to develop testing capabilities at Cal Poly to further investigate this technology.

1.1 Objective

The goal of this thesis is to use computational analysis to develop an approach for experimental investigation of circulation control wings that can be performed at Cal Poly.

Historically, experimental measurements for circulation control wings have been inconsistent and imprecise due to complex flow features and the small physical size of the jet. Aided by computational fluid dynamics (CFD) an approach for experimental data collection was created that will provide consistency and more targeted results from wind tunnel testing. The CFD results provided give insight into structural design parameters, performance aspects of the wing that were overlooked during the design phase, as well as instrumentation type and placement.

1.2 Methodology

First, a circulation control wing was designed that is capable of being tested in the Cal Poly Low Speed Wing Tunnel (CPLSWT). The purpose of designing for the CPLSWT was to have on-site capabilities to continually improve experimental techniques for circulation control wings. The design of the wing was an iterative process going through design and analysis cycles in order to meet the designated requirements detailed in Chapter 2.

CFD models were created using Star CCM+. The wing was modeled in a simulated wind tunnel with bounding walls the same dimensions as the CPLSWT as well as a freestream domain. This allows the impact of the wind tunnel walls to be demonstrated. Due to the high

computational resource demand of a full 3D CFD model, 2D CFD models were utilized to simplify the analysis. The impacts of this decision will be discussed in Chapter 5

The generation of a sufficiently refined mesh was completed using Star CCM+. To ensure the mesh was sufficiently refined, a mesh convergence study was completed. The specific details of the mesh generation process are detailed in Chapter 3.

The solvers used for the CFD model were guided by previous analysis on circulation control wings. There will always be the opportunity for more detailed analysis, but it must be balanced with computational expense. Since the purpose of this thesis is to determine experimental design considerations for wind tunnel testing, it was desirable to develop a CFD model that accurately modeled the jet flow. The jet flow is typically where the highest level of uncertainty arises in experimental environments. A highly refined mesh in the wake region along with higher order solvers were required for this goal. This is further detailed in Chapter 4. To ensure the CFD is correctly modeling the flow physics, a validation run was completed. This compared previous experimental data to the current CFD model.

After all the CFD simulations were run on the Cal Poly Bishop HPC, the data was analyzed and post processed to provide insight for experimental testing. Data was collected from the CFD models that can also be measured during wind tunnel testing. This includes surface pressures, field pressures, force and moment coefficients, velocity flow fields, along with streamline visualization.

1.3 Theoretical Considerations

1.3.1 Circulation

Circulation is a key tool in understanding the calculation of aerodynamic lift. If a curve C exists in some velocity field, as in Figure 2, V and ds are the velocity and direction of the line segment at some point on C. The circulation, Γ, is shown by equation 1.1.

$$\Gamma = -\oint_c V \cdot ds \tag{1.1}$$

Circulation describes a kinematic property of the flow field that is solely dependent on the velocity field and the selection of the curve C. [1]

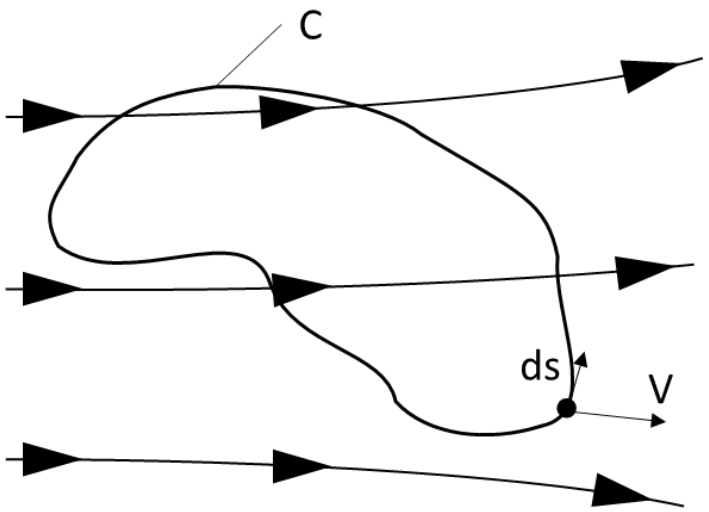

Figure 2. Curve C in the velocity field. The point on curve C shows the components for V, the streamwise direction and ds, normal to the curve C.

When this concept is applied to a lifting airfoil the resulting circulation can be seen in Figure 3. It should be noted that curve A, surrounding the airfoil, has positive finite circulation while curve B, containing just the freestream flow, has circulation equal to 0.

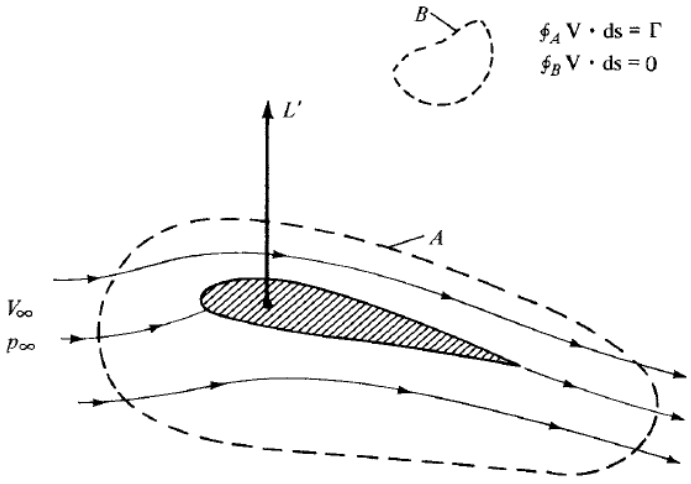

Figure 3. Circulation of curve A, surrounding a lifting airfoil is a positive finite number and curve B, in the far-field freestream flow is exactly 0. [1]

Vortex flow is fundamental in explaining lifting flows. For vortex flow, all the streamlines are concentric circles about a given point, as seen in Figure 4. The velocity magnitude along each

streamline is constant, and varies between streamlines inversely proportionally to the distance from the center, r. For a simple vortex flow around a point, like in Figure 4 it has been proven that circulation is constant between all streamlines. [1] From this property, the strength of a vortex flow is defined by the circulation around a streamline.

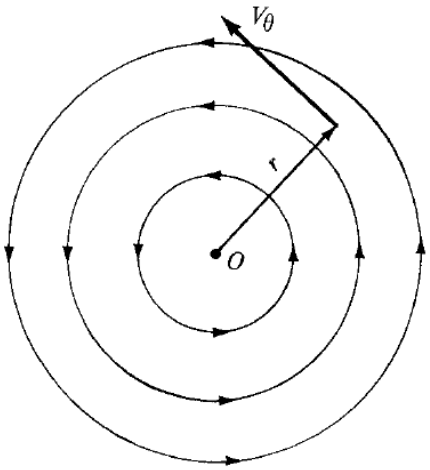

Figure 4. A vortex flow about point O having strength Γ [1]

To better understand how circulation relates to lift, flow over a circular cylinder is investigated and can be seen in Figure 5. This figure shows the inviscid incompressible solution for flow over a circular cylinder with an added vortex of strength, Γ. The reason to investigate the inviscid solution is to determine the theoretical maximum lift that can be created through the induced forces from circulation control. In reality, this theoretical maximum is never reached due to viscous effects and boundary layer separation on typical objects. However, with active pneumatic control, this theoretical maximum can be approached by controlling the boundary layer and the total circulation. Pneumatic control entails any type of blown or sucking jet from the body surface.

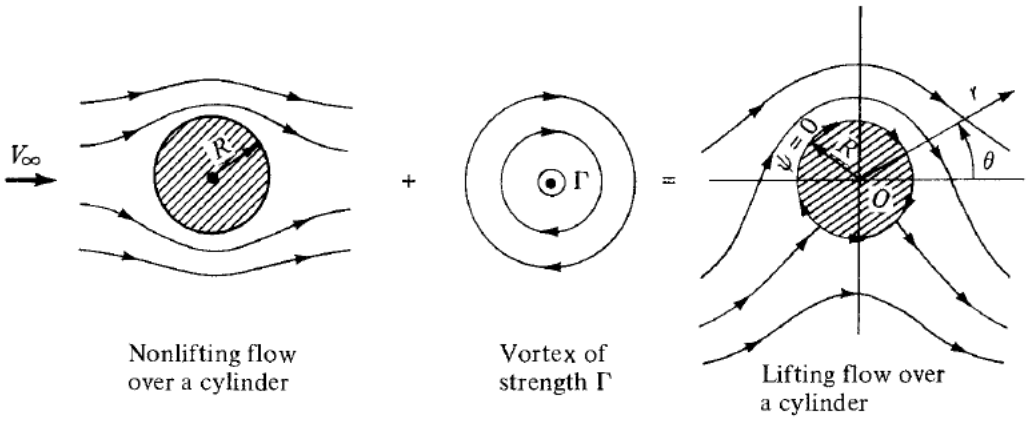

Figure 5. Synthesis of lifting flow over a cylinder [1]

It should be noted that as the circulation intensity increases, the stagnation points on the circular cylinder move closer together along the bottom surface, until they meet. At this point the streamlines see an impact which can be seen in Figure 6. Technically, it is possible to exceed this point and have the stagnation points leave the body such as with Flettner rotors, but this is not a good analog for an airfoil which has the stagnation points on the body.[1]

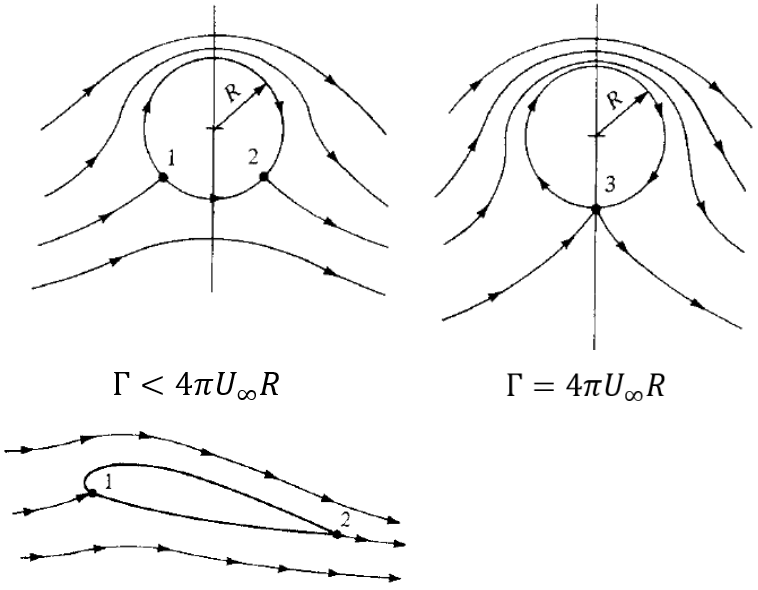

Figure 6. Stagnation point locations (points 1, 2, and 3) and circulation on a circular cylinder and an airfoil shape with their corresponding circulation values [1]

The Kutta-Jukowski Theorem, equation 1.2, demonstrates the relationship between circulation and lift per unit span.

$$L' = \rho_\infty U_\infty \Gamma \tag{1.2}$$

If the circulation is set equal to the theoretical maximum from the inviscid analysis, the following substitution is possible to solve for the lift force per unit span (L').

$$\Gamma = 4\pi U_\infty R \tag{1.3}$$

$$L' = \rho_\infty U_\infty (4\pi U_\infty R) \tag{1.4}$$

$$L' = \rho_\infty {U_\infty}^2 (4\pi R) \tag{1.5}$$

This lift force per unit span can then be converted into the lift coefficient.

$$C_L = \frac{L'}{0.5\,\rho_\infty {U_\infty}^2 D} \tag{1.6}$$

$$C_L = \frac{\rho_\infty {U_\infty}^2 (4\pi R)}{\rho_\infty {U_\infty}^2 R} \tag{1.7}$$

$$C_L = 4\pi \tag{1.8}$$

It is finally shown that the maximum lift coefficient for a circular cylinder is 4π.

1.3.2 Lift and Drag with Powered Lift

Figure 7 shows the circulation control wing that was designed for this project with the key variables listed.

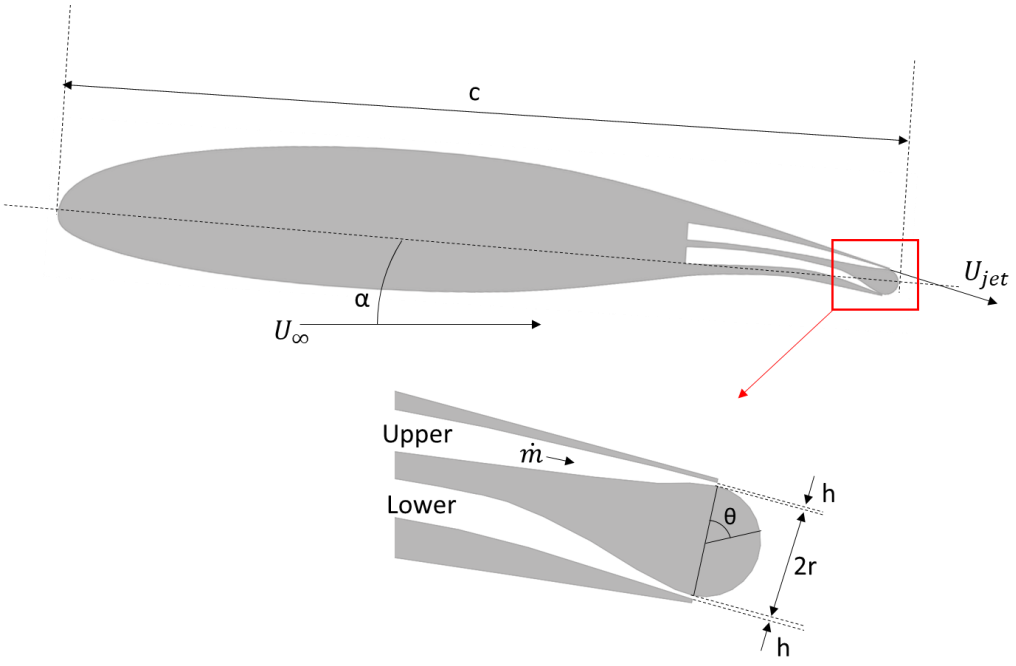

Figure 7. Key variables used for circulation control problems

Where, c is airfoil chord, α is angle of attack, U_∞ is freestream velocity, U_{jet} is jet velocity, $\dot{m}$ is the mass flow rate of the jet, h is the jet slot height, r is the Coanda surface radius, and θ is the jet separation angle. The model shown here is capable of upper and lower slot blowing.

There are two main force considerations for pneumatic powered lift devices: induced forces due to circulation, and reaction forces due to jet momentum. [7] The addition of a pneumatic system adds an additional circulation component from the reactionary forces of the jet. This creates 2 circulation terms: Γ_c and Γ_{jet}, where Γ_c is the induced circulation term and Γ_{jet} is the jet reaction circulation term. Using these, a new form of the Kutta-Jukowski Theorem can be formed as equation 1.9

$$L' = \rho_\infty U_\infty \left(\Gamma_c + \Gamma_{jet} \right) \tag{1.9}$$

Where

$$\Gamma_{jet} = \frac{\dot{m}\, U_{jet}}{\rho U_\infty} (\alpha + \delta) \tag{1.10}$$

Where α is angle of attack of the airfoil and δ is the jet exit angle relative to the chord line. This equation can be related to the jet component of lift and drag coefficients with:

$$C_{L\,jet} = C_T \sin(\alpha + \delta) \tag{1.11}$$

$$C_{D\,jet} = C_T \cos(\alpha + \delta) \tag{1.12}$$

Where $C_T = \frac{\dot{m} U_{jet}}{qS}$ which is the thrust coefficient for the jet. It can be seen from these equations that the jet will produce either lift or drag depending on δ and α. Figure 8 shows an example of a typical pure jet flap and a circulation control airfoil with their corresponding δ. For a pure jet flap, most of the lift improvements come directly from the jet reaction force. However, with circulation control almost all the jet reaction force is in the form of thrust. The key improvement provided with circulation control is the increase of induced forces due to the streamline turning from the Coanda surface, which typically allows circulation control airfoils to provide larger overall lift benefits than a pure jet flap. [7]

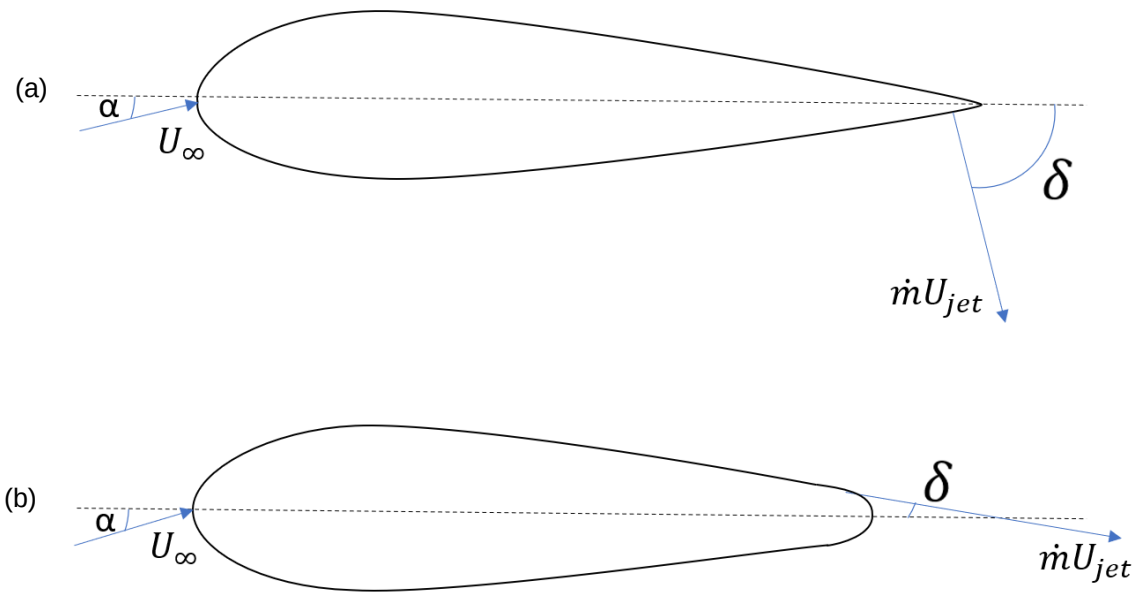

Figure 8. A jet flap airfoil (a) and a circulation control airfoil (b) showing the difference in typical jet exit angle (δ).

One of the most important aspects of testing and recording data from circulation control experiments is accurately measuring the momentum coefficient (C_μ) represented in equation 1.13. Momentum coefficient represents the thrust force from the jet normalized by the freestream dynamic pressure and wing area.

$$C_\mu = \frac{\dot{m}U_{jet}}{qS} \tag{1.13}$$

Where $\dot{m}$ is represented by equation 1.14

$$\dot{m} = \rho_{jet}U_{jet}A_{slot} \tag{1.14}$$

Historically, there has been recorded difficulty in measuring momentum coefficient accurately and consistently. [7,8,9,10,11,12] The difficulty in accurately measuring this quantity experimentally has led to efforts to quantify momentum coefficient in different ways. [11] These methods should be noted when reviewing this paper and performing future experiments. Typically, isentropic expansion to freestream conditions is used to calculate U_{jet} which can be seen in equation 1.15. It should be noted that $\dot{m}$ and U_{jet} can be directly measured and controlled in CFD simulations, but this is difficult in an experimental setting without disrupting the flow field.

$$U_{jet} = \sqrt{\frac{2\gamma RT_{plenum}}{\gamma - 1}\left(1 - \left(\frac{P_\infty}{P_{plenum}}\right)^{\frac{\gamma}{\gamma-1}}\right)} \tag{1.15}$$

Isentropic expansion assumes that the flow is inviscid and that it fully expands to freestream pressure. In reality there is a boundary layer that forms in the jet exit and the jet will expand to the local pressure surrounding the jet exit. However, isentropic expansion to freestream pressure has been shown through previous studies [11] as well as the results in Chapter 5 of this paper to model the jet velocity well enough for this situation. The jet velocity is dominated by the plenum pressure ratio $\frac{P_\infty}{P_{plenum}}$. This becomes a useful performance quantity to evaluate various circulation control systems. A visual representation of the measured variables are shown in Figure 9.

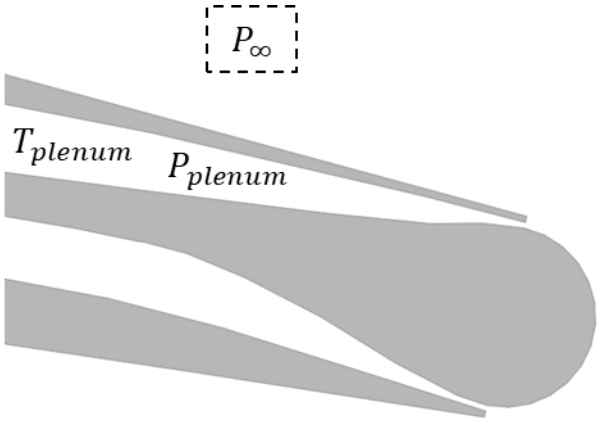

Figure 9. Defining the variables needed to calculate jet velocity using isentropic expansion.

It can be useful for circulation control problems to define an $C_{D\,EQ}$ due to the added momentum from the jet flow. A simple force based correction will be used for this paper as seen in equation 1.16. When performing experimental testing a force balance will measure the thrust impact of the jet. Hence, to avoid negative drag values the force component of the jet reaction is accounted for.

$$C_{D\,EQ} = C_{D\,bal} + C_\mu \cos(\delta + \alpha) \tag{1.16}$$

Where $C_{D\,bal}$ is the drag coefficient as seen by a force balance.

A kinetic energy based correction has also been proposed previously. [8] This is more useful for comparing different types of powered lift devices, and incorporates the cost of accelerating the jet flow. This is represented by equation 1.17.

$$C_{D\,EQ} = C_{D\,bal} + C_{\mu}\left(\frac{U_{jet}}{U_{\infty}}\right) \tag{1.17}$$

It has been shown that the kinetic energy term dominates the $C_{D\,EQ}$ term at higher momentum coefficient values. This tends to hide the thrust benefits from circulation control and will not be utilized herein.

Chapter 2

BACKGROUND

2.1 History of Circulation control

Circulation control has been extensively investigated since the early 1960's. [4] One of the original focuses was on rotorcraft blades to improve lift performance. [4] Around the same time investigations were also started to see how this concept could be applied to aircraft wings. In the late 1970's the first flight demonstrator, an A-6A with a circulation control wing modification, was flown on a test flight shown in Figure 10. There were promising results that came from this: a 60-65% reduction in takeoff and landing distances, and CL improvements of 120% over conventional Fowler flaps. [4] These results were promising, but some of the main issues still present were the additional drag in cruise flight caused by the blunt trailing edge and carrying an onboard air source.

Figure 10. Modified Navy/Grumman A-6A aircraft with circulation control being tested in 1977 [17]

The poor cruise drag performance was the next issue to be tackled. The original A-6A test flight had a trailing edge radius of 3.65% r/c. DTNSRDC and Grumman tried modifying the trailing edge shapes of the circulation control wing to improve the cruise drag performance. [4] They modified a typical super critical airfoil to employ circulation control. It was found that with a small enough (0.018c) trailing edge radius they were able to maintain the lift improvements while greatly decreasing the drag penalty in cruise. [18] The drag penalty, even with the small radius

trailing edge, was still significant for an aircraft in cruise. However, this shows an important trend: it is possible to maintain most of the high lift benefits with a small trailing edge radius thereby significantly decreasing the drag penalty.

Circulation control had a popularity peak in the 1980's and there were a lot of different applications tested including: powered lift and engine thrust deflection, propellers, as well as many non-flying applications like tractor trailers. Varying levels of success came from these ventures, with none maintaining longevity in development. [4]

Engler also mentions the use of circulation control to improve control authority. [4] A test was conducted using a full aircraft model and only activating the circulation control on half of the span. By doing this a large roll moment was created due to the lift differential. The results from this test can be seen in Figure 11. They also investigated using circulation control blowing at the wing tip, which further improved the performance due to increasing the effective wing span.

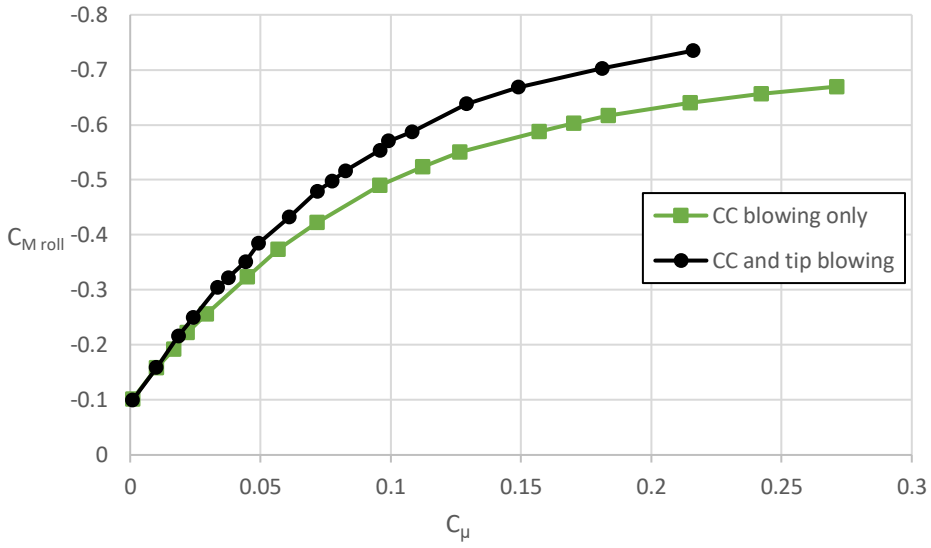

Figure 11. This plot shows the effect of momentum coefficient on rolling moment for a CCW blowing on half the span. It also shows the impact of tip blowing. The maximum roll moment coefficient is about -0.7 at a momentum coefficient of .25 [4]

The results from this test demonstrate significant control authority with only circulation control. According to the study, tip blowing further increased the roll moment as well as decreased drag by extending the effective aspect ratio. The plot showing the drag reduction is shown in Figure 12.

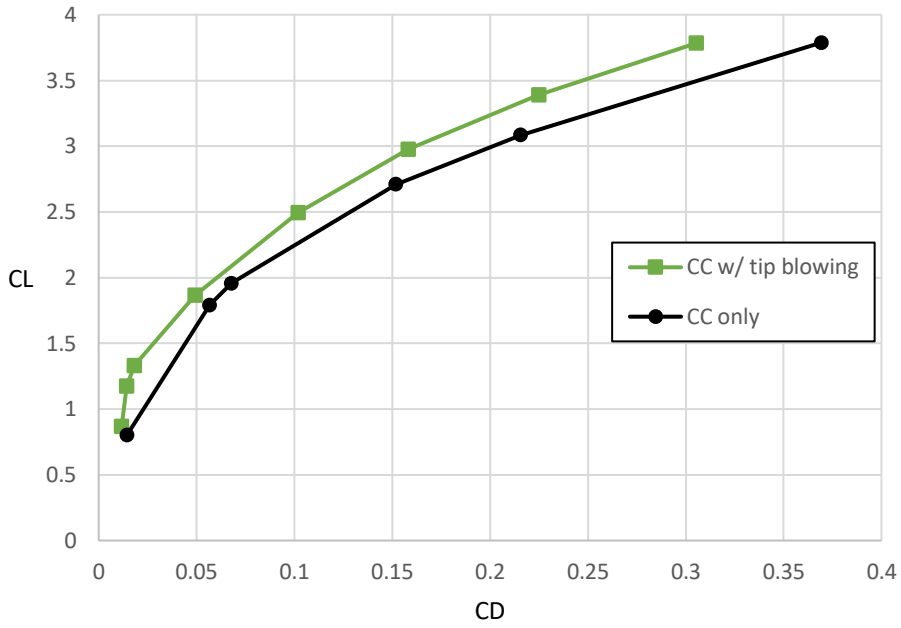

Figure 12. Drag polar showing circulation control only and with added tip blowing.[4]

The historical study of circulation control wings has provided valuable insight in trailing edge design noting that smaller trailing edge radius can maintain the high lift benefits while reducing unblown cruise drag. Control authority using circulation control wings has also been demonstrated in wind tunnel testing, showing the potential to use circulation control wings as a complete or partial replacement for mechanical control surfaces.

2.2 NASA General Aviation Circulation Control Wing

In more recent developments, NASA completed wind tunnel testing of a circulation control wing named the General Aviation Circulation Control (GACC) wing seen in Figure 13.[8] This was conducted at NASA Langley Research Center in the Basic Aerodynamic Research Tunnel (BART). This is an open return wind tunnel with a 42” square test section. This is similar in size and capability to the Cal Poly Low Speed Wind Tunnel. This experimental data set provided a candidate to validate the CFD model due to the geometric and kinematic similarity between this test and the model developed for the current project.

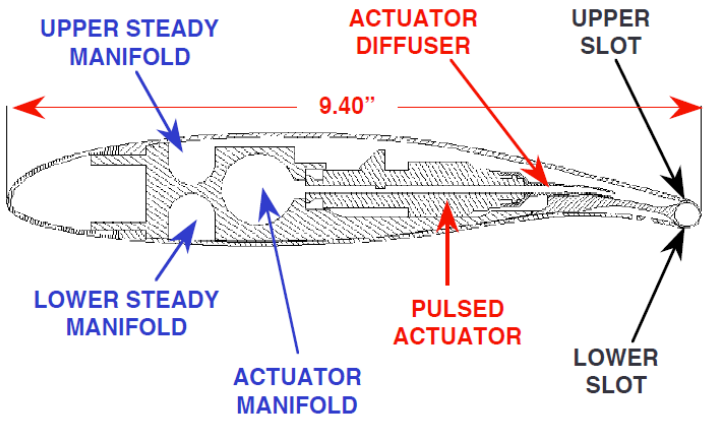

Figure 13. 2-Dimensional 17% Low Speed General Aviation Circulation Controlled Airfoil with a circular trailing edge r/c: 2% [8]

It is important to note that this experiment was performed as a 2D test where the wing spanned the entire test section. There were a lot of valuable conclusions produced from this testing campaign. One of the unique capabilities of this wing was that it had independent upper and lower blowing. Lower surface blowing acts like deflecting a mechanical control surface upwards, with a decrease in lift. When both upper and lower blowing were activated simultaneously it was shown a “pneumatic trailing edge” was created and greatly reduced the drag produced. The reduction in drag relative to the cost of the momentum coefficient required is highly dependent on the specific geometry, momentum coefficient ratio, and freestream flow conditions. Overall, this technique was found to significantly improve the equivalent L/D in cruise conditions up to 65 compared to . [7] The equivalent L/D values that were reached with dual blowing were not quite as high as the clean airfoil with an unmodified trailing edge, but it proves that dual blowing is a valid solution to improve cruise performance. The drag values were corrected according to the equivalent drag described in equation 1.17.

The GACC model had the capability to swap the trailing edge shape. It was determined the circular trailing edge shape reached a significantly higher $C_{L\,MAX}$. The elliptical shape had the best cruise drag performance at higher speeds due to the increased thrust produced, [7] but this came at the cost of much higher momentum coefficients to produce the same C_L.

The GACC testing data has been used previously for CFD validation. [9] A summary of the work NASA completed in the early 2000’s was compiled by Jones et al. [9] They mostly

focused on 2D simulations. Typically, CFD over-predicted lift, with the over-prediction increasing as the momentum coefficient increased. [9]

It was noted here and in other papers that one of the difficulties in validating CFD results came from measurement uncertainty involved with the jet flow. [12] The two key parameters are the jet velocity profile and jet slot height. These are both involved in calculating the momentum coefficient. Due to the physical scale of the jet being very small (~0.01”) it was reportedly difficult to accurately measure these values without error values that were considered significant in the calculations. There was span-wise variance up to 20% in the jet velocity in the experimental testing. In addition to this, the jet slot height may change up to 20% when the plenum is pressurized. [7] It was noted that the slot should be measured before and during operation. In addition to this, the structure of the wing and supports for the slot are important to maintain a consistent slot height throughout testing. A hotwire probe has been used to measure the jet slot exit velocity along with pressure sensors in the plenum. Using a hotwire probe was determined to be too invasive to utilize during testing. It was also recommended that more care be taken to equalize the span-wise velocity profile in the plenum design.

One more attribute that was noted from the NASA 2D wind tunnel tests was a significant vortex that forms due to a full span model intersecting the tunnel walls, which can be seen in Figure 14. [9] In a 2D CFD simulation, these vortices are not simulated. In a real wind tunnel test, these vortices can lead to significant measurement error if not accounted for.

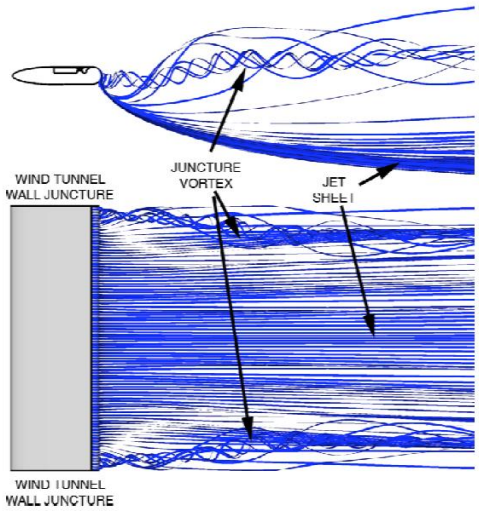

Figure 14. 3D CFD simulation of a full span circulation control wing in a wind tunnel with visible wall juncture vortices forming [9]

The impact of these wall juncture vortices could make it difficult to analyze the data with high confidence. Even without blowing, there is a necklace vortex that would form along the wall juncture, but this would remain constant at a given angle of attack. Therefore, it is possible to isolate the impact of varying momentum coefficient from the impact of the wall vortex by utilizing partial span blowing. Partial span blowing simulates an outboard portion of a wing utilizing circulation control.

2.3 AMELIA

The AMELIA project was a full aircraft model with dual radius circulation control flaps, leading edge blowing slots, engine simulators, and advanced instrumentation. [10] This was tested in the NASA AMES NFAC 40'x80' wind tunnel. An image of the model with smoke flow visualization is shown in Figure 15. This is a complex model with a lot of specific design decisions that make some of the data difficult to extrapolate to general circulation control cases.

Figure 15. AMELIA model in the NASA Ames 40'x80' wind tunnel with smoke flow visualization showing the streamline turning from the active circulation control. (NASA.gov)

Until the AMELIA project was completed, a majority of the CFD validation efforts had been focused on 2D cases. [3] This is largely due to the difficulty in accurately quantifying the full 3D extent of the experimental results in the detail needed for high confidence validation. This includes the complex juncture flow at the outer ends of the blowing slot, cross flow components, as well as the typical difficulties in accurately measuring momentum coefficient across the whole span. One of the main goals from the AMELIA project was to create a data set for future 3D CFD validation efforts. The results from this test do include one of the most thorough quantifications of 3D circulation control wind tunnel tests. [10] It should be noted that the AMELIA project was designed for a specific end goal - Cruise-Efficient Short Takeoff and Landing (CESTOL), for airliner scale aircraft.

The AMELIA project experimentally tested one specific type of circulation control trailing edge design: the dual radius flap which can be seen in Figure 16. This design requires mechanical control to rotate the flap during operation. The benefits from this design come from the high-speed cruise performance, which is almost identical to an unmodified non-CC airfoil. This limits the use of circulation control to solely high lift situations as well as increasing mechanical complexity. Previous 2D tests using the GACC wing have shown potential for

simultaneous upper and lower blowing on a blunt circular trailing edge to be used to create a pneumatic trailing edge as well as a pneumatic control surface. Based on the information available at the time of writing, the AMELIA project did not seem to investigate this technology.

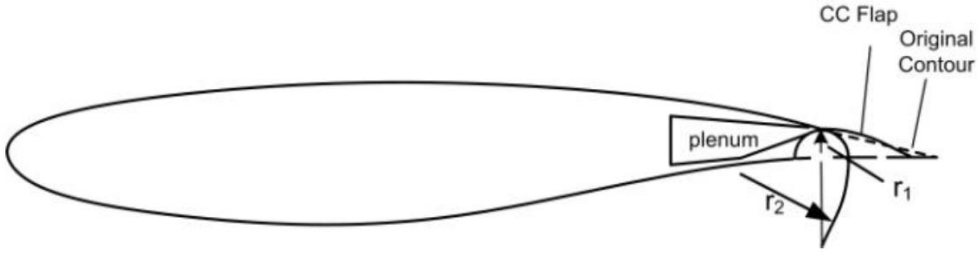

Figure 16. An example of a dual radius flap circulation control wing

One more finding in the AMELIA testing was contradictory to previous research. [10, 12] In previous research before the AMELIA testing it was shown that dual radius flaps with circulation control had improved lift performance when set to 90° versus 60°. However, in the AMELIA testing it was discovered that the dual radius flap had a higher $C_{L\,Max}$ in the 60° configuration. This discrepancy highlights the difficulty in relying on previous circulation control research without carefully investigating the methodology used and the specific design of the test article.

2.4 Summary

In summary, there is a great foundation of knowledge about circulation control wings with even more to still investigate. There has been consistent difficulty in accurately measuring momentum coefficient for CFD validation purposes, so the results from previous research must have the experimental methods considered in depth before relying on the results. There have been wind tunnel tests, flight tests, and CFD done previously, all showing very promising results for this technology. The design space has not been fully investigated to optimize performance. Planning and executing well documented experimental testing of 3D circulation control wings will provide valuable insight into the effectiveness of this technology.

The range of parameters investigated through the GACC study were $C_\mu < 0.1$, r/c=2%, and h/c=0.0014 and 0.0022.

Chapter 3

WING DESIGN

The purpose of this wing is to isolate the performance of circulation control on a generic rectangular wing. This will provide valuable insight into this technology to improve the performance capabilities of PAVs or UAVs, which are similar in physical scale to a small general aviation aircraft. Previous research has shown that circulation control wings provide the largest increase in lift per momentum coefficient at airspeeds closer to typical GA aircraft. [7] This is partly due to the increasing mass flow requirements as airspeed increases. PAVs and some UAVs have requirements for short takeoff and landing capabilities, strict noise restrictions, and efficient cruise. [7] Employing designs similar to current general aviation aircraft will get vehicles to market more rapidly and reduce cost. The specific wing design for this project utilizes concepts from previous testing that have proven effective. The aforementioned air vehicles typically cruise at a chord Reynolds Numbers on the order of 10^6.

3.1 Requirements

The model shall have the capability to test in the CPLSWT. There have been previous wind tunnel testing efforts to quantify the capabilities of circulation control wings, however many of the efforts have been incomplete. It is valuable to produce general 3D circulation control wing data in a controlled environment with a focus on improved measurement techniques.

The test article shall be a 3D wing. The purpose of this is to expand on the previous 2D wind tunnel testing that was completed and gather more data on a generic 3D circulation control wing. Wing tip effects and the root juncture of the blowing span are of particular interest.

The testing shall be capable of reaching a chord Reynolds Number $\geq 1x10^6$ for the wing. This provides dynamic similarity to typical PAV and UAV. This is important to provide accurate results especially with the high level of boundary layer interaction with the jet flow.

The model shall have upper and lower blowing capabilities. This gives the wing the capability to provide roll control, reduce cruise drag, as well as act as a high lift system.

The airfoil shall be capable of sectional lift coefficients ($C_{L\,MAX}$) of 5. This is a preliminary upper limit value intended to provide data for a large range of lift coefficients and to determine what is feasible to experimentally investigate with the equipment accessible at Cal Poly.

The model shall have a fixed trailing edge shape. This requirement is an effort to simplify the design of the wing. The benefits of not having any mechanical control surfaces have the potential to reduce aircraft weight.

3.2 Initial Design Process

The GACC test model developed by NASA provides a baseline for the design. There has been significant wind tunnel testing done on the 2D GACC model at the LaRC by jones et al. This provides a set of data that can be used for CFD validation as well as a performance baseline.

A 17% low speed airfoil, the LS(1)-0417 GA(W)-1 was modified at the trailing edge to create the Cal Poly Circulation Control (CPCC) airfoil profile as shown in Figure 17. The top surface of the wing was unchanged, the bottom surface of the wing was modified aft the 75% chord location. This modification location was selected based on the GACC airfoil design. [8] One of the reasons for selecting this airfoil profile was due to the large leading-edge radius which alleviates the large negative peak pressure coefficients and can be used as a substitute for a mechanical leading edge device by delaying leading edge separation and airfoil stall to high angles of attack. [7] Flow separation near the leading edge has consistently been an issue with circulation control wings, however it has been experimentally confirmed that a large leading edge radius will help delay flow separation. [7] Using this airfoil instead of leading edge blowing or a mechanical surface further simplifies the design, which is one of the goals of this project. The airfoil thickness allows for more significant internal structure as well as a higher theoretical $C_{L\,MAX}$.

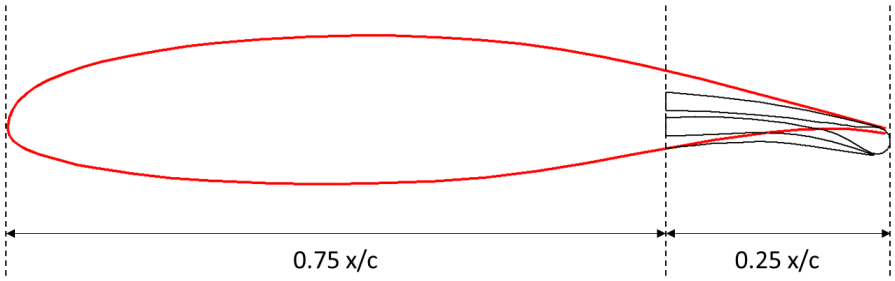

Figure 17. The original LS(1)-0417 GA(W)-1 profile in red and the modified CPCC airfoil in black with a 1.5% r/c circular trailing edge

The radius and shape of the Coanda surface impact both $C_{L\,MAX}$ and cruise drag. One of the requirements of this project is to have a fixed trailing edge shape. That means the dual radius design, like the one used in the AMELIA model, does not meet the requirements due to the mechanical rotation of the Coanda surface during operation. With the trailing edge shape fixed, a circular trailing edge generates the largest $C_{L\,MAX}$ improvements. [7]

The unblown drag was approximately equal at cruise conditions of all the trailing edge shapes investigated, however the circular trailing edge had the highest max L/D. [7] The circular trailing edge did have more drag in the blown configuration, but this effect can be lessened with a "pneumatic trailing edge". [7] In this context a pneumatic trailing edge is referring to blowing the upper and lower slots simultaneously at a specific ratio to improve the pressure recovery aft of the wing. [7] There are complex performance tradeoffs for the trailing edge shape that have not been fully investigated including potential weight reduction, mass flow requirements, and jet reaction thrust. This requires more detail for a full aircraft design, but the data collected herein provides a good starting point for that analysis.

In an attempt to minimize cruise drag, 3 different Coanda surface radii were tested: 1%, 1.5% and 2% r/c. When operated at $C_\mu = 0.2$ oscillations of 10% were observed in the 1% r/c solution, seen in Figure 18, that were independent of mesh size. This implies there is either

unsteady wake shedding at certain blowing parameters or the solution did not converge correctly. It is believed this trailing edge radius was too small to maintain streamline turning of the flow coming off the trailing edge of the airfoil. This behavior looks similar to flow over a circular cylinder with Von Karmen vortex shedding modeled in a steady state simulation. [6] It is also possible that this effect comes from the CFD incorrectly modeling some portion of the jet flow.

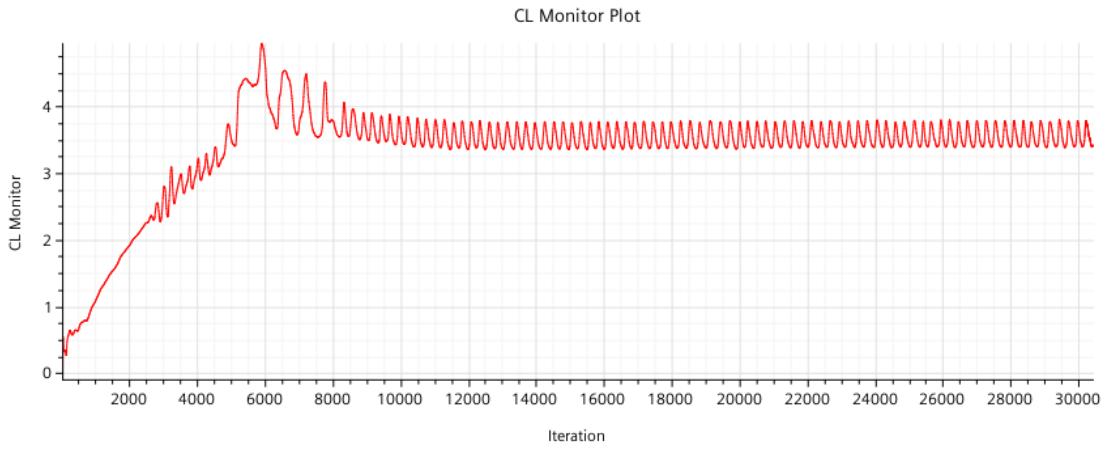

Figure 18. Lift coefficient monitor for the 1% r/c trailing edge design. Oscillations that do not damp out are approximately 10% of the value.

It was noted that pressure fluctuations in the jet wake were visible which can be seen in Figure 19. This unsteady wake shedding behavior would far outweigh any drag reduction gained by reducing the trailing edge radius. Due to this phenomenon, be it computational or physical, the 1% r/c trailing edge was not further investigated.

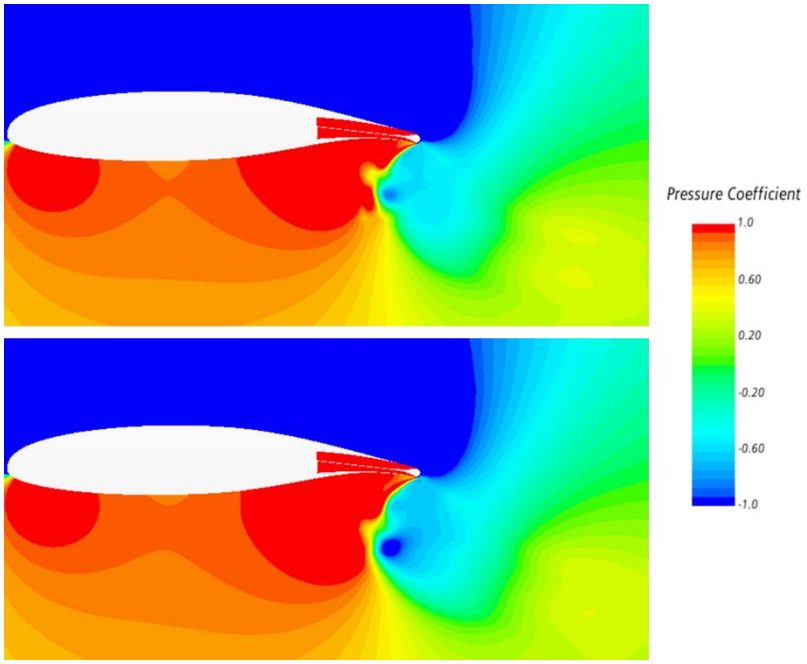

Figure 19. Pressure coefficient scenes 100 iterations apart in the steady oscillation region. (a) has a lift coefficient of 3.43 and (b) has a lift coefficient of 3.52

The trailing edge was increased in size to 1.5% r/c, which did not exhibit this unsteady wake shedding behavior. Comparing to a 2% r/c trailing edge, there is no reduction in C_L at $C_\mu = 0.2$. However, the 1.5% r/c trailing edge reduced the unblown drag by 23% compared to the 2% r/c. Based on this, the 1.5% r/c trailing edge was selected for further investigation. It should be noted for future research that trailing edge size and shape optimization can likely bring further performance enhancements.

One of the requirements of the design was to reach a chord Reynolds Number of $1x10^6$. The nominal maximum velocity of the CPLSWT is 40 m/s. This led to a chord length of 15 inches, which should allow for a maximum Reynolds Number of just above $1x10^6$. This effort to match the Reynolds number to a typical flight Reynolds number is an attempt to more accurately capture how the boundary layer develops and interacts with the circulation control flow. This large chord model will also help with manufacturability of the small circulation control components like Coanda radius and slot height due to their dependence on chord length.

The test article was required to be a 3D model to better understand the 3D flow effects occurring with circulation control. The objective for the test article is to have a way to isolate the

impact of an outboard circulation control panel. This was done by designing a root mounted wing section with a free tip that is further described in Section 3.3. The advantage of this over the previous 2D experimental testing is this will show how the wingtip and slot root vortices impact the L/D_{eq} of a circulation control wing. Slot root vortices form at the inboard section of a circulation control panel on a wing due to the stepwise change in lift along the span of the wing.

A solid blockage calculation was done before deciding on this chord length. With the span (b) at 26”, the solid blockage produced at an angle of attack of 12° is ~5%. This is deemed acceptable for this test based on guidance from Barlow et al. [2] Wake blockage, jet blockage, and streamline turning effects must also be considered for circulation control wind tunnel testing. Quantifying these corrections will be further discussed in Chapter 4.

The specific design of the plenum and the jet exit are shown in Figure 20. Some of the key parameters shown here are the trailing edge radius (r) and the slot height (h). Theta (θ) is the jet separation angle where 0° is completely separated and 180° is fully attached. Based on the chord length of 15” the ratio of Coanda radius to chord is 1.5%. The slot height ratio h/c= 1%. This slot height ratio was selected based on the GACC test data where it was demonstrated that this ratio gave the best performance while minimizing the mass flow rate requirement. [7]

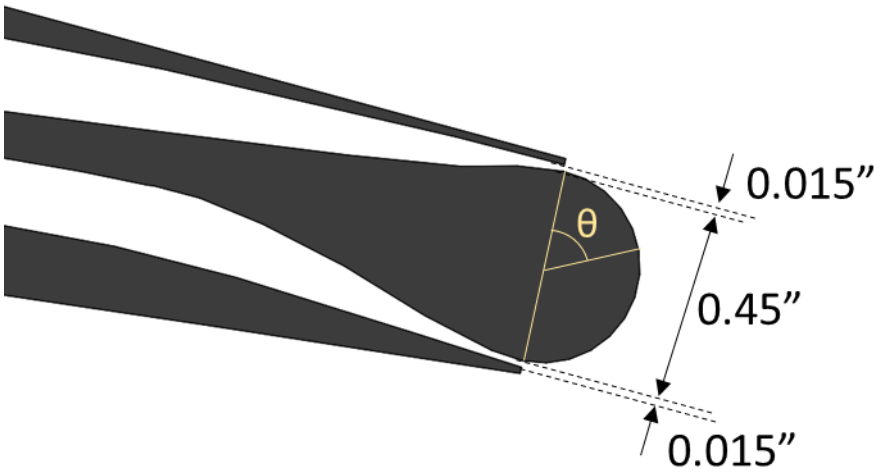

Figure 20. Detail view of the plenum and trailing edge of the CPCC airfoil. The upper and lower blowing slots are independently controlled.

The contraction ratio from the plenum to the exit is approximately 20. A detailed structural analysis was not completed for this portion of the project, however the aerodynamic loading produced from the CFD simulations are noted in Chapter 5 and provide a good starting point for future structural analysis.

3.3 Test Article

The final outer mold line design has been completed for this project. The detailed design of the internal structure for the wind tunnel model is left for the next phase of this project. However, designing with the eventuality of instrumentation and construction was kept in mind. A cross sectional view of the CPCC airfoil can be seen in Figure 21.

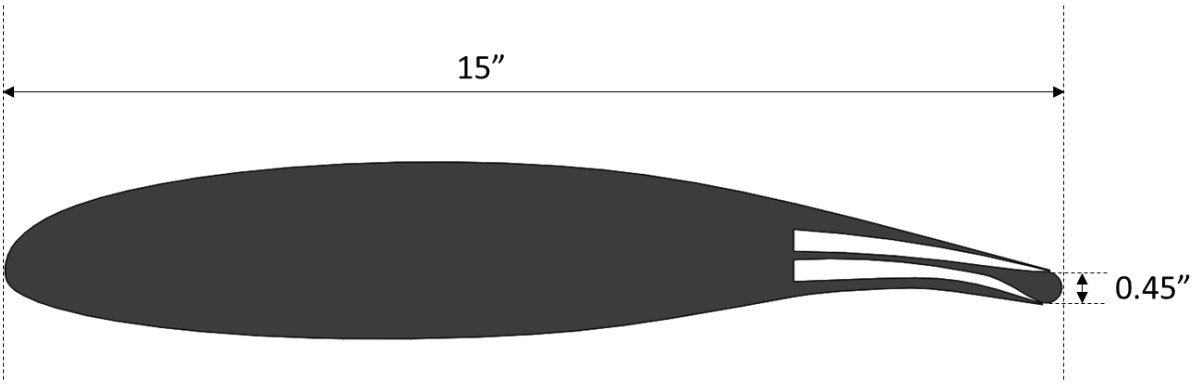

Figure 21. Cross sectional view of the CPCC airfoil with a 15” chord and a 0.45” (1.5% r/c) diameter circular trailing edge and independently controlled upper and lower blowing.

The CPCC wing model has partial span blowing which can be seen in Figure 22. It was noted that wall juncture vortices form when circulation control blowing is active along the entire span out to the tunnel walls.[9] These juncture vortices are much more intense than the typical necklace vortices that form at the root of a wing. This could impact the ability to isolate the effect of the circulation control blowing. To combat the influence of the wall interference, a 12” portion with no blowing at the root (shown in red) is designed. This places the 12” portion of the span with blowing (b_{blown} shown in green) in the center of the wind tunnel domain. A 2” end cap (shown in red) is on the outboard tip of the wing. This is necessary to structurally support the blown slot. It will be noted from the analysis of the results that it may be necessary to extend the blown slot length due to the juncture vortices that form. This will be further discussed in Chapters 5 and 6.

The overall aspect ratio for this wing is $^{26}/_{15}$ which is relatively small for a typical wing. However, the purpose of this test article is to act as a “semi-infinite” wing, wherein there is only 1 free tip and the root is acting as “infinite”. This design mitigates the negative impact of having a low aspect ratio wing and focuses the research on the circulation control blowing and the wing tip effects.

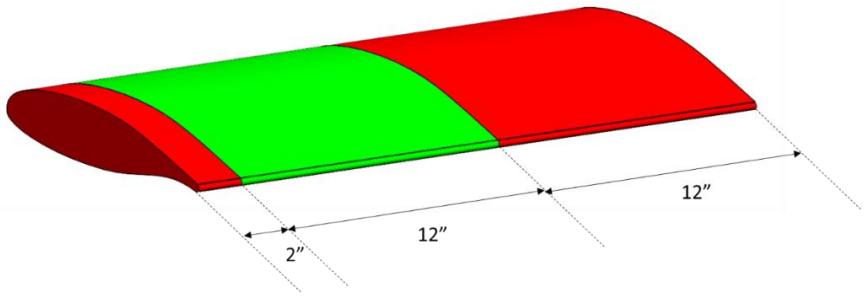

Figure 22. Isometric view of the 3D CPCC wing. The green portion represents the area with active circulation control blowing and the red portion has no blowing.

The wing can be seen in the CPLWST domain in Figure 23. The tip of the wing has 10” between the tunnel wall, which provides space for the outboard the wing tip vortex to form. Based on the preliminary 3D CFD shown in Chapter 5, this distance should be sufficient. The wing is centered horizontally in the tunnel to minimize the impact the tunnel walls have on the jet wake.

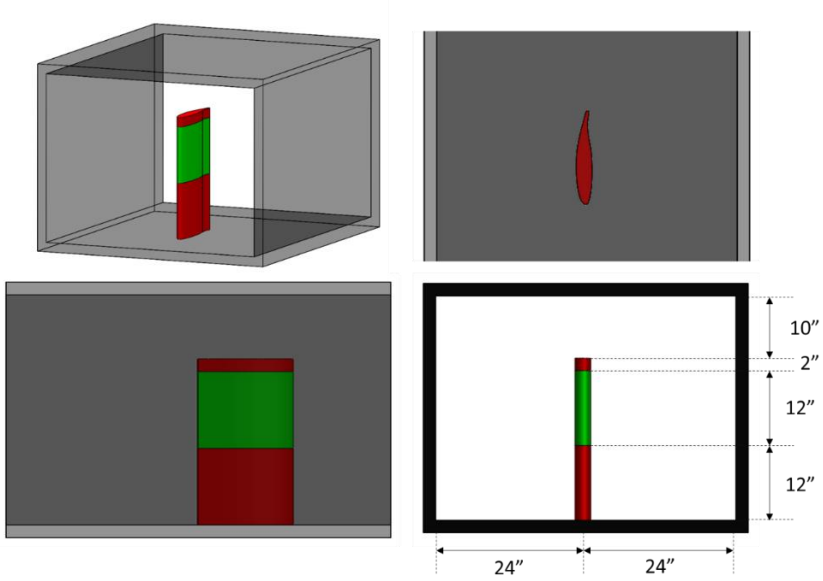

Figure 23. 3-view and isometric model of the CPCC wing in a representation of the 48”x36" CPLSWT test section

The aspect ratio of the slot, $b_{blown}/h = 800$, is a more important parameter for this test than the wing aspect ratio. The juncture of the blown and unblown sections create increasingly intense vortices as C_μ increases due to the sharp change in lift along the span of the wing. These vortices decrease the $\Delta C_L/C_\mu$ similarly to wing tip vortices decreasing L/D. Most of the previous research has been on 2D models which assume an infinite span b_{blown}, so there is not much experimental data available relating to slot aspect ratio for circulation control. The results from the 3D CFD results in Chapter 5 demonstrate how significant these vortices are. It is valuable to investigate this phenomenon experimentally due to the difficulty in accurately numerically simulating that flow regime.

3.4 Validation Model

A replica of the GACC model was created to validate the CFD results which can be seen in Figure 24. The GACC airfoil was a good candidate for CFD validation due to the large amount of 2D wind tunnel data collected throughout the testing of the GACC model and the similarity to the current design. Only the upper blowing slot was modeled for the validation case. It was assumed that if the upper slot blowing could be modeled correctly, then other circulation control blowing would also be modeled correctly. This method of simplifying the physical model for the CFD simulation is a common way to reduce computational time. It was noted from later simulations including both slots that this did not have a significant impact on the results, but did improve convergence time.

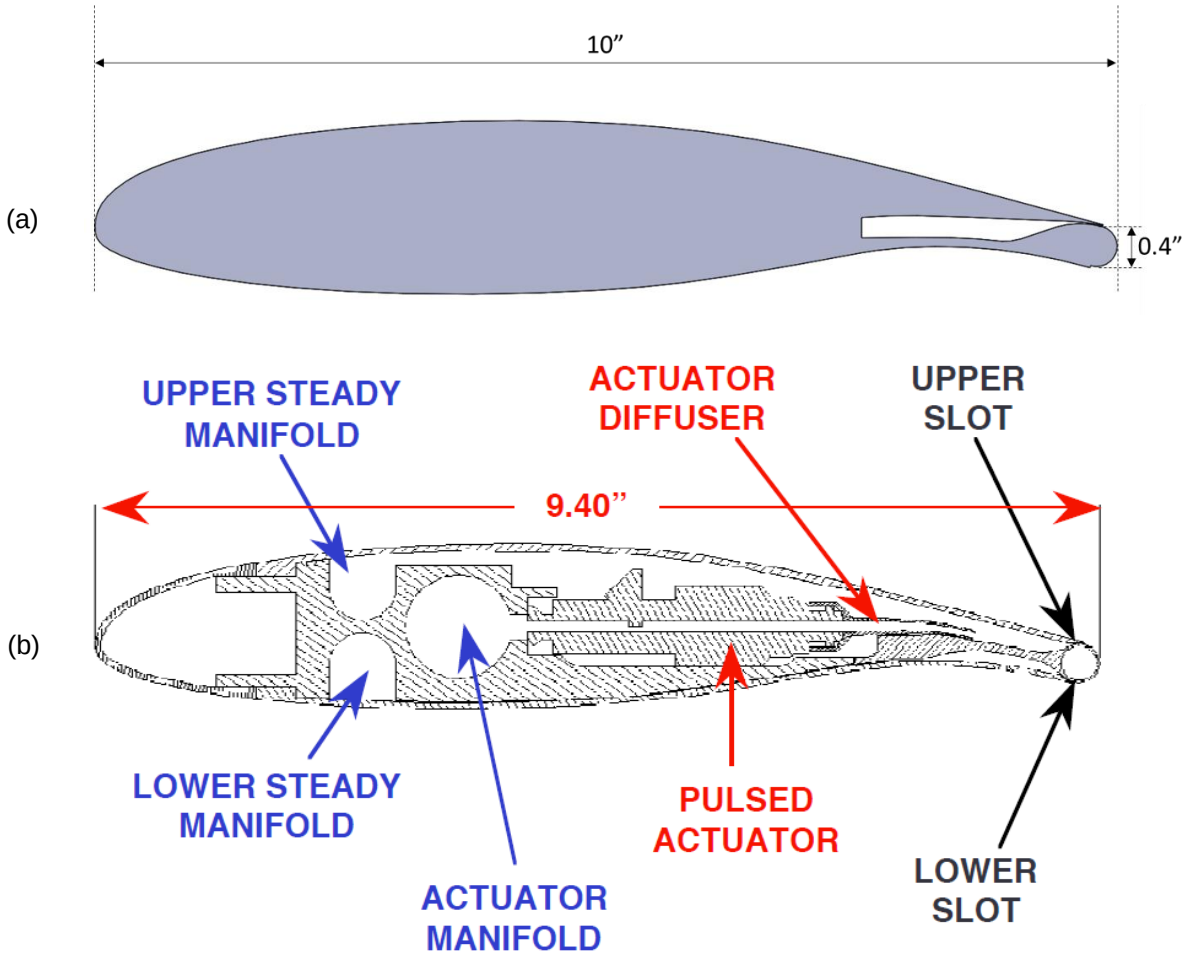

Figure 24. The replica created for CFD validation (a) with a 10” chord and a 2% r/c circular trailing edge and the original GACC airfoil (b) with a 9.4” chord and a 2% r/c circular trailing edge.

The same method of modifying the LS(1)-0417 (GA(W)-1 airfoil was used to create the replica as documented for the original GACC airfoil. The top surface of the airfoil was left untouched, but a new bottom surface line was created from 75% chord back to the bottom the circular trailing edge. Section 4.4 details the CFD results from the validation study.

Chapter 4

CFD MODELING

Analysis of the CPCC wing was accomplished by utilizing CFD. Numerical analysis was used to evaluate the process of experimentally investigating a circulation control wing. The CFD model was validated against previous experimental data to provide higher confidence the circulation control flow was captured correctly.

The simulations were run on the Cal Poly Bishop High Performance Computer (HPC). The Bishop HPC has 240 processor cores, specifically 20x Intel Xeon E5-2650v4, 2.2GHz (12-Core, HT, 30MB Cache, 105W) 14nm. The HPC also has a total of 1.1 Terabytes of RAM. Graduate students at Cal Poly have access to 96 processor cores at a time which can be split between different jobs, with a single job using a maximum of 24 cores. The setup of the simulations were done locally on a laptop. 2D CFD simulations were the main focus due to the extreme resources required to accurately simulate a 3D circulation control problem. This will be further discussed in the meshing section.

A progression of various models were simulated throughout this project. The GACC validation model was created first to ensure the CFD model was accurately capturing the 2D flow physics. This was a 2D case and was used for validation as well as the mesh refinement study. After that, the 2D version of the CPCC airfoil was modeled to collect higher density data points. Finally, a full 3D model was simulated at a representative condition with inadequate results for in-depth analysis. The 3D simulation was able to provide some qualitative impacts that will provide insight to future wind tunnel testing.

4.1 Geometry and Domain

Once the 2D and 3D geometric models were created in SolidWorks, they were imported to Star CCM+ as IGES files. The different surfaces are separated so they can be individually controlled by the automatic parts-based meshing. The 2D models act as full span blowing with no

3D effects. This will be valuable in determining sectional parameters for experimental design. The 3D wing model is exactly as shown in Chapter 3.

With the geometric model of the wing imported, now a fluid volume must be created. Typically, with CFD there is a domain sizing study done, but due to the fact this simulation is mimicking a wind tunnel test, the domain is constrained to those dimensions. The CPLSWT test section has a cross section of 36”x48”. The wing will be oriented vertically so the span extends parallel the 36” length wall. This gives the maximum distance for the wake to dissipate before impacting the side walls. The inlet was placed 80” upstream of the wing to allow similar tunnel wall boundary layer growth to the CPLSWT. The outlet was placed 100” downstream of the wing leading edge to allow for adequate dissipation before reaching the pressure outlet. A cross sectional view of the 2D CPCC model is shown in Figure 25.

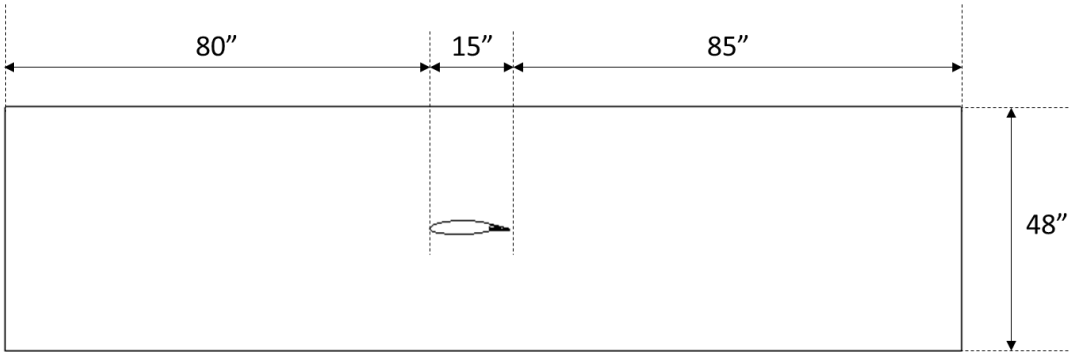

Figure 25. A cross sectional view of the 2D fluid domain used for the Star CCM+ simulations. The same domain size and leading edge locations were used for the GACC validation cases.

Once the domain was sized and created, the solid wing was subtracted from the fluid volume. At this point, each of the previously named surfaces were assigned to different regions, which allows the user to specify the physical aspects of that surface. Note Table 1 labeling the boundary type of each surface.

Surface	Boundary Type
Tunnel inlet	Velocity inlet
Tunnel outlet	Pressure outlet
Tunnel walls	No-slip walls
Wing surfaces	No-slip walls
Plenum inlets	Mass flow inlets

Table 1. Boundary types for the region assigned to each part surface.

The wind tunnel walls were assigned as no slip walls to capture the boundary layer growth along the length of the wind tunnel. It was also desirable to measure the pressure distribution on the tunnel wall. The tunnel inlet is a velocity inlet, and the outlet is a pressure outlet. The upper and lower plenum inlets are assigned as mass flow inlets. The rest of the wing surfaces are all no slip walls.

The 3D model geometry was created in a similar fashion and an isometric drawing of the domain can be seen in Figure 26. The main difference in creating the 3D domain was the need for all of the tunnel walls. As mentioned previously the cross section of the wind tunnel domain is 36”x48”. The same length for the tunnel domain was used for both the 2D and 3D models.

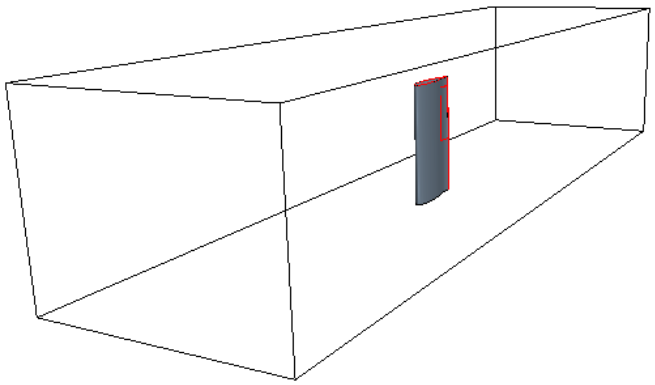

Figure 26. Wireframe outline of the 3D wind tunnel domain with the CPCC wing.

4.2 Physics Model and Solvers

The physics conditions and solvers were set next. Some of the key focuses of modeling circulation control were capturing the flow at the jet exit, the wake dissipation, and the separation behavior from the Coanda surface. The jet flow induces streamline turning and causes a shear layer between the jet and the flow coming from the trailing edge. The simulations were steady state Reynolds Averaged Navier Stokes (RANS). For future research it would be valuable to investigate unsteady simulations as well to better capture the time dependent effects.

The Coupled implicit flow model solves the conservation equations for mass, momentum, and energy simultaneously. [18] The 2nd order upwind discretization scheme was selected. The reason for selecting the coupled implicit flow solver is the improvement in solving compressible flow problems. Higher momentum coefficient values lead to sonic flow at the nozzle exit, which is highly compressible. The air was modeled at standard sea level conditions as a compressible ideal gas. This is similar to the typical conditions seen at the CPLSWT.

Turbulence modeling and boundary layer development modeling has a significant impact on circulation control numerical analysis. It has been discussed that CFD typically over-predicted lift for circulation control wings.[9] Some of the reasons hypothesized for this are incorrectly modeling the jet exit flow and the boundary layer development over the Coanda surface. [18] The viscous regime is modeled as fully turbulent, which is recommended for this type of problem due to the difficulty in accurately predicting boundary layer transition. [18] The K-ω SST turbulence model was selected for this study because it has been shown to model the complex flow and streamline turning well. [18] Star CCM+ has built in improvements to the turbulence model such as compressibility corrections, 2nd order convection, and a quadratic constitutive relation which further improved the accuracy of the solution.

A low wall y+ treatment was used for all the simulations because it was desired to fully resolve the boundary layer. This is necessary to accurately model the flow over the Coanda surface because of the strong interaction of viscous, pressure, and centrifugal forces that keep

the flow attached. For this to be effective, a prism layer mesh with a y+ value of approximately 1 must be implemented. The details of this are further explained in Section 4.3.

4.3 Mesh

Creating a high-quality mesh is important to capture the flow effects of the circulation control wing. In the beginning of this project the extreme computational demand to accurately simulate 3D circulation control problems was underestimated. The main issue comes from the blowing slot being so small compared to the wing chord. Since the slot height to chord ratio, h/c, is about 0.1% this creates a large demand for mesh refinement near the blowing slot and the Coanda surface. As previously discussed, accurately characterizing the jet at the nozzle exit is one of the most difficult parts about testing and simulating circulation control. To get an accurate velocity profile at the jet exit, it was recommended to have at least 5 cells in the core of the jet flow. It is not desirable to grow adjacent cells too quickly or else artificial diffusion may occur. This leads to very demanding meshing requirements, especially in the 3D case where this effect is further amplified.

All meshes were created using the Star CCM+ automatic parts-based meshing. This is a tool that allows for specific volumetric and surface refinement. First a surface mesh is created based on the geometry parts. Then, a volume mesh is built on top of that.

A trimmed mesh was used because it converged to a solution more rapidly than a corresponding polyhedral mesh with similar accuracy. A trimmed mesh uses predominantly hexahedral cells with minimal cell skewness. Based on an informal initial study, the trimmed mesh has more cells than a similar polyhedral mesh. However, due to the more desirable orientation and skewness of the cells, the solution converged more quickly. Since they have similar accuracies for these types of problems, the convergence time was deemed the deciding factor.

Prism layers were added to all of the wall surfaces on the wing and the tunnel walls to capture the boundary layer. A wall y+ of 1 demonstrates the prism layers are sufficiently refined to capture the velocity and shear stresses in the boundary layer. A representation of the prism layers on the Coanda surface and jet exit can be seen in Figure 27. Wall y+ values are

dependent on the local flow velocity, so the prism layers had the near wall thickness decreased and the total number of prism layers increased near the jet exit where high speed flow was present. With these modifications a y+ value of approximately 1 was obtained on the Coanda surface and jet surfaces.

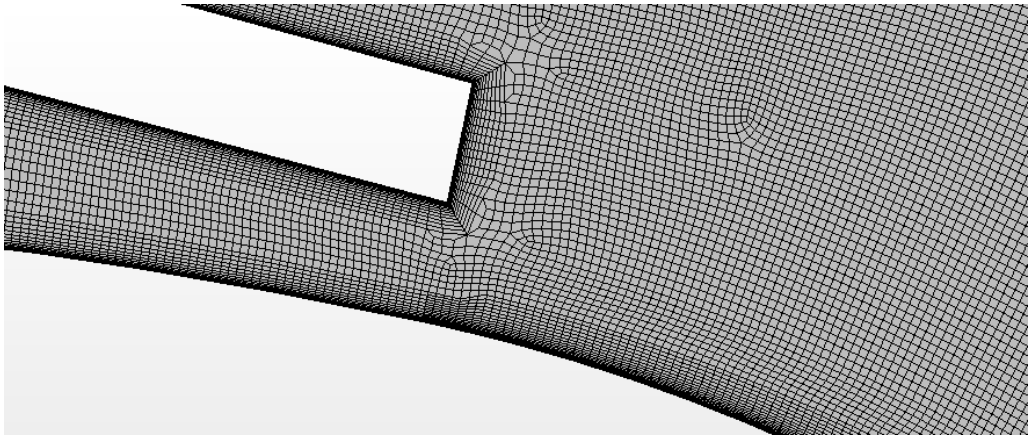

Figure 27. Detail view of the upper slot exit showing the prism layers bounding all of the wall surfaces.

The initial mesh was generated on the GACC validation model and a representation can be seen in Figure 28. 3 rectangular prisms were created for volumetric refinement which provides higher levels of control on the mesh refinement. The largest volume surrounds the airfoil to capture the flow over the wing surface. There is another refinement region around the Coanda surface to capture the jet turning. The last volumetric refinement region extends downwards to capture the wake of the jet flow. Measurements were taken on an initial simulation to ensure these refinement regions extend to capture the full jet wake.

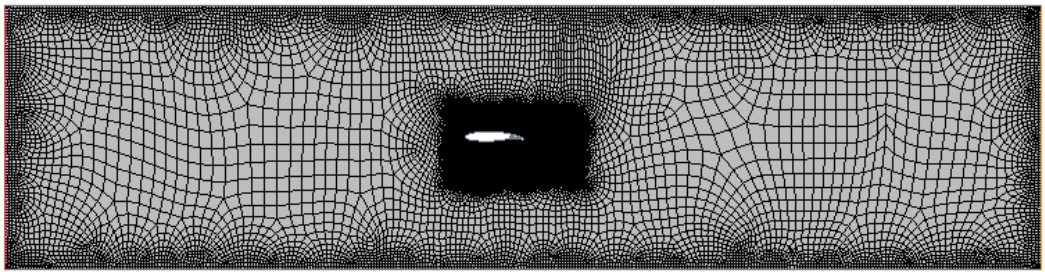

Figure 28. Medium density mesh set up for the 2D GACC validation case containing 1.7 million cells.

A total of 3 levels of mesh refinement were tested to show mesh independence. The total number of cells in each mesh refinement can be seen in Table 2.

Mesh refinement level	Coarse	Medium	Fine
Number of cells	500k	1.7 mil	5 mil

Table 2. Mesh refinement levels for each mesh used in the mesh independence study

The mesh independence study was done at the maximum momentum coefficient being investigated of approximately 0.3. This provided sufficient mesh refinement for the most extreme case tested. It should be noted that the momentum coefficient is not directly set, a mass flow rate for the plenum is set and the momentum coefficient is determined by probing the slot exit velocity, which can be seen in Figure 29. There are 500 discrete measurement points, which allow a full velocity profile to be determined at the slot exit location.

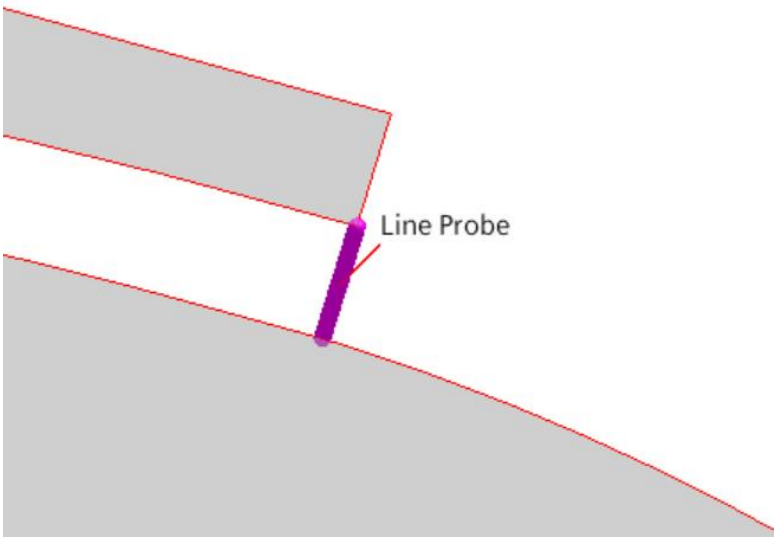

Figure 29. The line probe that was used to measure the exit jet velocity. There are 500 discrete measurement points to capture the full boundary layer velocity profile.

The location of the line probe is kept constant through all the simulations to ensure consistency in the measured value. The mass flow rate for the plenum was set to 0.5 lb/s for all the simulations. The results for the lift and momentum coefficients are shown in Table 3.

Mesh Refinement	Coarse	Medium	Fine
C_L	5.03	4.65	4.73
C_μ	0.326	0.321	0.322

Table 3. Lift coefficient (C_L) and momentum coefficient (C_μ) results for mesh refinement study

This table shows that the medium and fine meshes have very good agreement, with the C_L within 2% difference. The coarse and medium meshes have approximately 8% difference in C_L. The momentum coefficients of all the cases are within 2% of each other. The medium mesh has greatly improved convergence time compared to the fine mesh, and using the grid convergence index referenced by Roache [18] the medium mesh only has 0.36% error. Based on this the medium mesh was selected with approximately 1.5 million cells.

This mesh was selected to use for all the 2D cases. There were some slight modifications made to the volumetric refinements as the results were interpreted for the validation case and applied to the CPCC airfoil. The wake refinement region was extended to fully capture the wake of the circulation control flow based on the results of the validation study. This helps mitigate as much artificial wake diffusion as possible. The change in volumetric refinement can be seen in Figure 30.

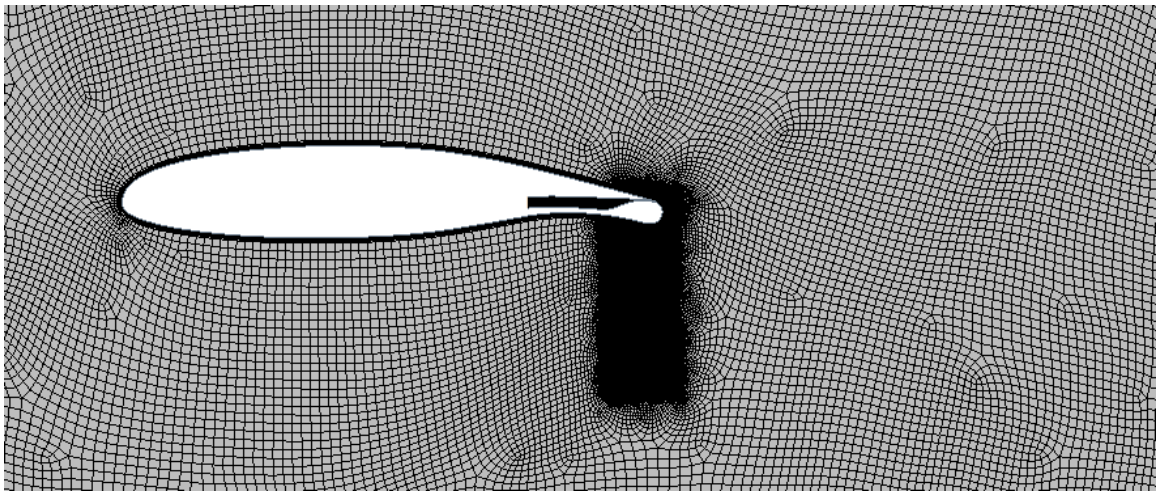

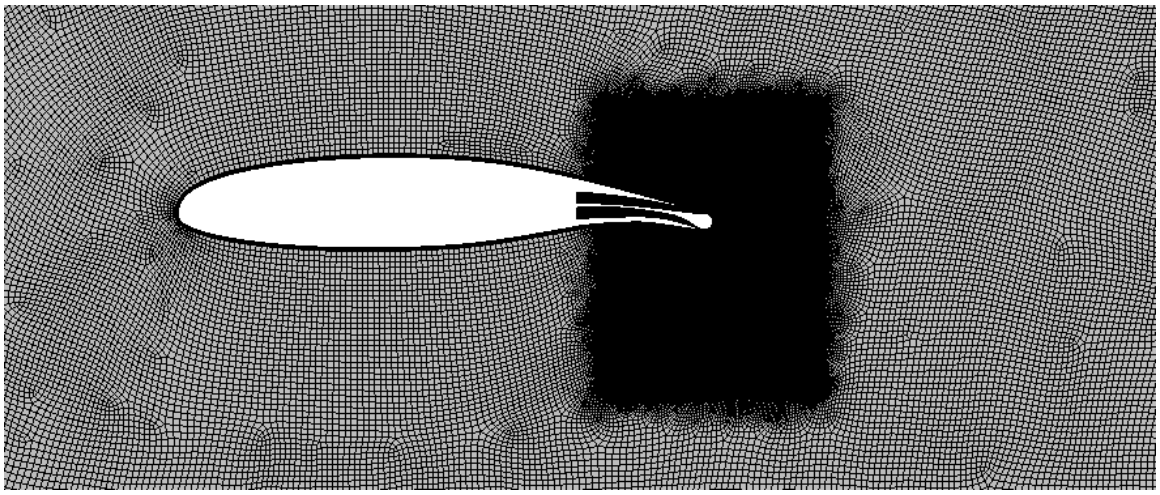

Figure 30. Progression of the wake refinement in the circulation control region.

For the 3D model, the mesh refinement was limited by computational expense. An attempt was made to create a 3D mesh with the same cross-sectional refinement as the medium 2D mesh. This was determined not to be possible on the current hardware due to memory limitations. Even if this mesh could be generated, it would likely be so large that it would take on the order of weeks or months to converge to a solution. It was determined that the maximum number of cells that could be feasibly be run on the hardware available was approximately 30 million with the desired size on the scale of 15 million cells. Other mesh optimization efforts for 3D circulation control problems have encountered similar issues with limited hardware capacity. [18] A cross sectional view of the mesh created for the 3D simulation is shown in Figure 31.

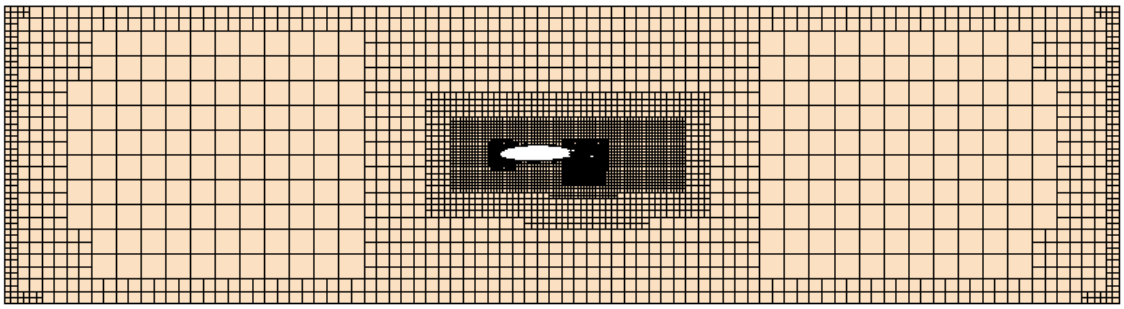

Figure 31. A cross sectional view of the 3D mesh containing 15 million cells

There are approximately 15 million cells in the 3D mesh generated. The cell density near the Coanda surface and jet exit is not as refined as desired, but were deemed sufficient to

provide a baseline in combination with the 2D data. A 2D cross section with the same refinement as the 3D case was created and compared to the validation data. The 2D cross section had approximately 50,000 cells, 30x less than the medium mesh refinement. This implies that a sufficiently refined 3D mesh could be up to 450 million cells, which is unreasonable on most available hardware. This demonstrates the need for further investigation into the 3D CFD cases either with better mesh optimization or more robust hardware.

4.4 Validation Case

The GACC wind tunnel test results are used in conjunction with the GACC replica CFD model that was created for this project to validate the CFD model. Details of the design and methodology used for the GACC wind tunnel testing are discussed in Chapters 2 and 3. The purpose of this validation is to show that the current CFD model is accurately describing the real-life flow physics. A sweep of momentum coefficients was completed from 0 to 0.1 because that was the available test data. A comparison of the wind tunnel test data and the CFD model can be seen in Figure 32.

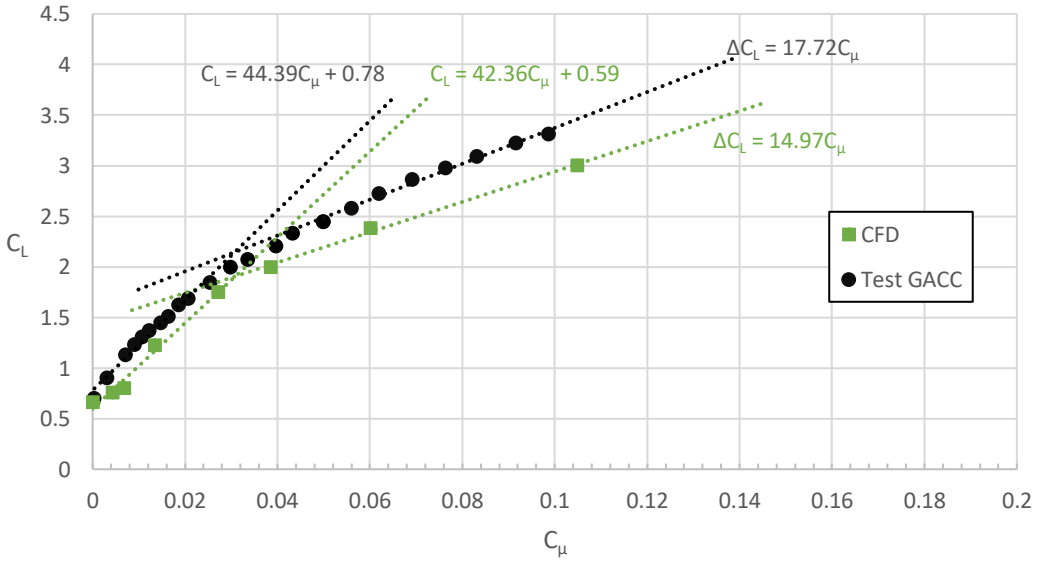

Figure 32. Momentum coefficient vs lift coefficient for the experimental GACC data and the CFD data with trend lines showing the boundary layer control and super circulation regions.

The CFD model and experimental data demonstrate decreasing agreement with increasing momentum coefficient. This is likely due to the error in measuring the momentum coefficient

experimentally increases with increasing momentum coefficient. It was noted in the data that measurements of the slot height and jet velocity had error values up to 20% at higher momentum coefficients. [7] The CFD data agrees within the experimental error levels. This gives confidence in the CFD model and provides insight into why further wind tunnel testing is valuable.

The two distinct linear regions, boundary layer control and super circulation control, are clearly observed in both sets of data. The two separate regions each have a linear slope where the datasets have an R^2 value greater than 0.98. The CFD data follows the same linear trends with the transition point from boundary layer control to super circulation occurring at the same momentum coefficient. This demonstrates the CFD correctly captures both circulation control flow regimes. The slopes in the boundary layer control region have approximately 4.6% difference while the super circulation control regions vary by 16.6%. Error increasing relative to momentum coefficient is explained again by the increasing experimental error. This level of agreement is within the associated experimental error and provides confidence in the CFD model.

Chapter 5

RESULTS

5.1 2D Results

Detailed analysis of the 2D CPCC airfoil provides valuable insight to the sectional characteristics of the wing. 2D simulations are less resource intensive than 3D simulations due to the simplified flow physics and smaller overall mesh size. This allows for more complete analysis to augment the 3D results. This 2D analysis provides insight into experimental testing for this airfoil.

5.1.1 Unblown Configuration

The CPCC airfoil with no blowing was simulated and compared to historical wind tunnel testing data for the clean baseline LS(1)-0417 (GA(W)-1 airfoil having no circulation control modification. This shows how the change in camber along with the blunt trailing edge impacts performance. The resulting lift coefficient versus angle of attack is shown in Figure 33.

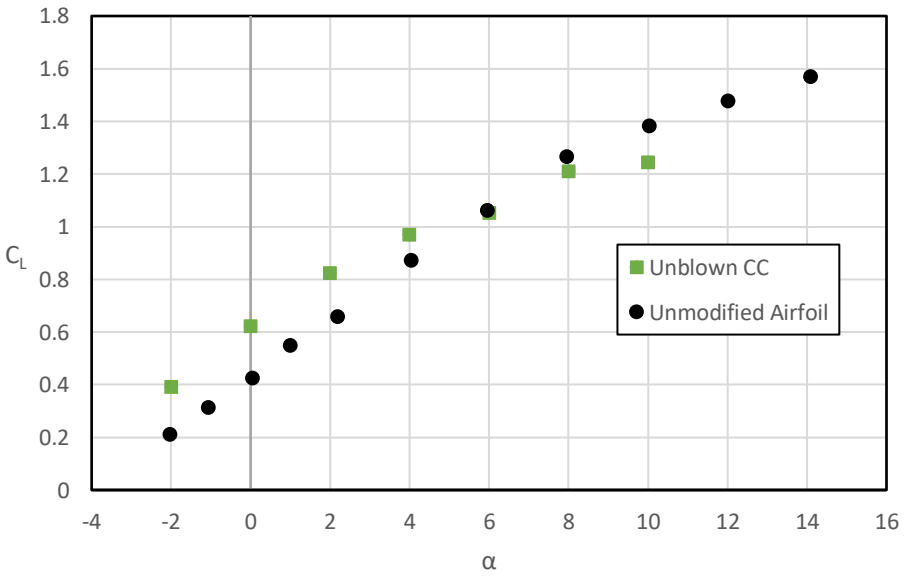

Figure 33. CL vs α plot for the unblown configuration compared to wind tunnel test data for the original LS(1)-0417 (GA(W)-1 airfoil with no circulation control. [13]

The drag polar for both the unblown CPCC airfoil and the baseline LS(1)-0417 (GA(W)-1 airfoil are shown in Figure 34. It should be noted at typical cruise lift conditions the unblown

CPCC airfoil produced approximately 17% higher drag compared to the original LS(1)-0417 (GA(W)-1 airfoil. This is to be expected from the circular trailing edge creating a larger wake of separated flow. Section 5.1.3 will demonstrate how the dual blowing configuration can modify the cruise efficiency.

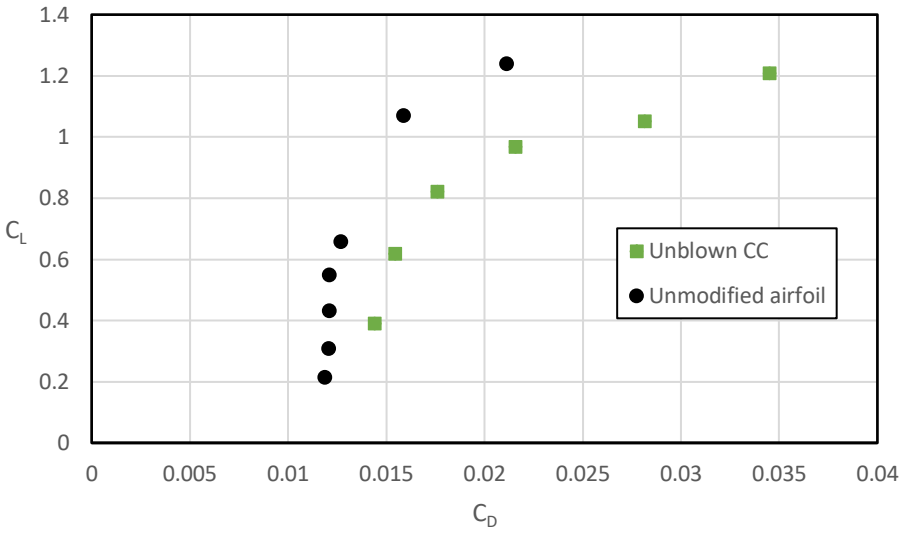

Figure 34. Drag polar for the original LS(1)-0417 (GA(W)-1 airfoil and the CPCC airfoil in the unblown configuration [13]

The pressure coefficient along the surface of the unblown airfoil at varying angles of attack are shown in Figure 35. This follows the typical pattern of unblown airfoils where the majority in ΔC_P occurs at the fore end of the airfoil. This causes the aerodynamic center to typically occur near c/4, which is the case here.

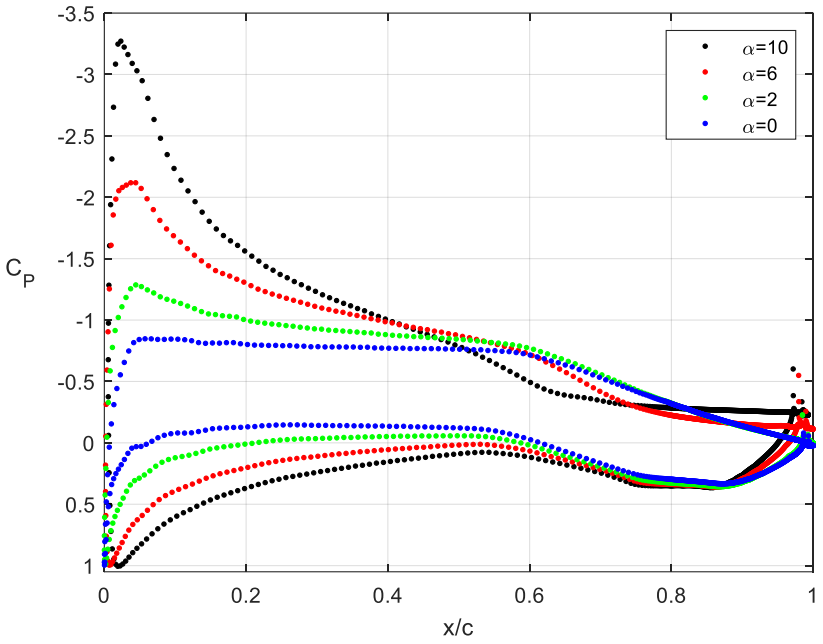

Figure 35. Pressure coefficient along the normalized wing surface for the unblown CPCC airfoil.

The unblown case can be treated like a normal wing section in a wind tunnel test. The only correction needed is the solid blockage [2] seen in equation 5.1.

$$\varepsilon_{sb} = \frac{0.9(model\ volume)}{(tunnel\ area)^{3/2}} \tag{5.1}$$

Further analysis to prepare for testing is not necessary for the unblown case, but this data presents a good performance baseline for the airfoil.

5.1.2 High Lift Configuration

The high lift configuration consists of blowing solely from the upper slot. Representative scenes at a C_μ of 0.012 and 0.152 are shown in Figure 36. These show the boundary layer control region and the super circulation region, respectively.

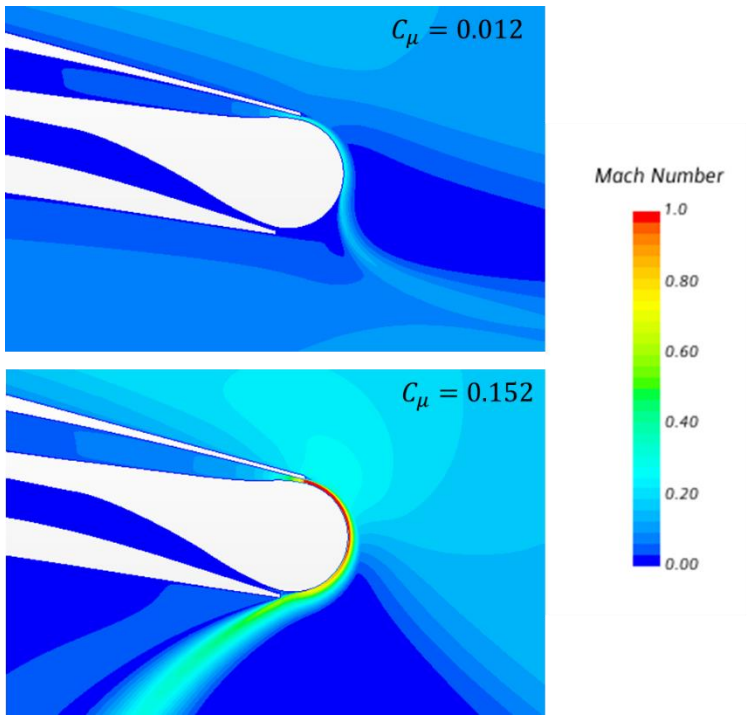

Figure 36. Mach scene at two different momentum coefficients demonstrating the boundary layer control and super circulation control regions. α=0°

The two distinct regions of flow for circulation control, boundary layer control and super circulation control, have different performance characteristics. It can be seen in Figure 37 that the ΔC_L is approximately 5x lower when operating in the super circulation region. This is important when analyzing performance characteristics for circulation control wings.

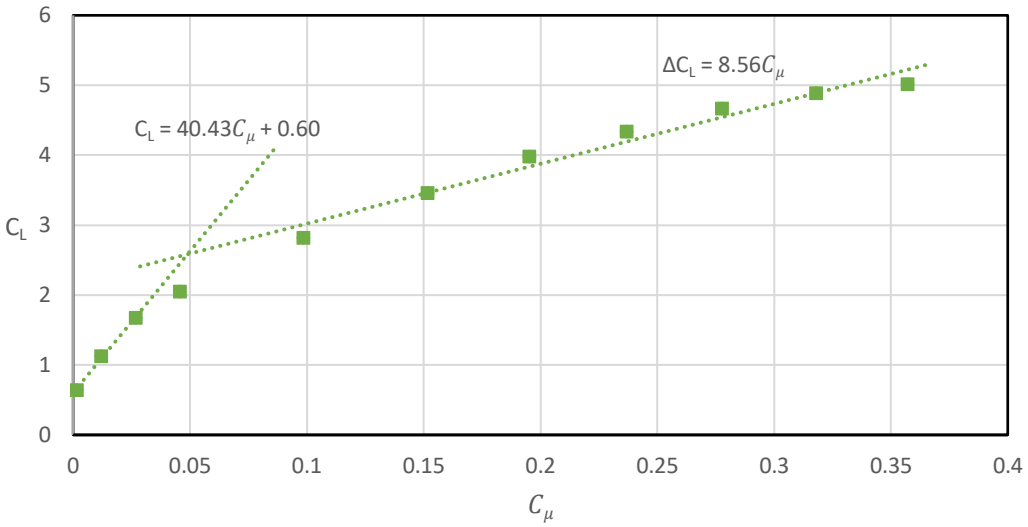

Figure 37. C_μ vs C_L for the CPCC airfoil at 0° AoA. The boundary layer control region and super circulation regions are denoted by the two trend lines. α=0°

The leading edge stagnation point moves aft along the bottom surface as C_μ increases as predicted in the theoretical analysis in Chapter 1. In the super circulation region this causes the flow along the upper surface of the wing to separate prematurely even at low angles of attack. In the boundary layer control region ($C_\mu = 0.012$) the flow remains attached to higher angles of attack. This is demonstrated in Figure 38 showing C_L vs α for different momentum coefficients.

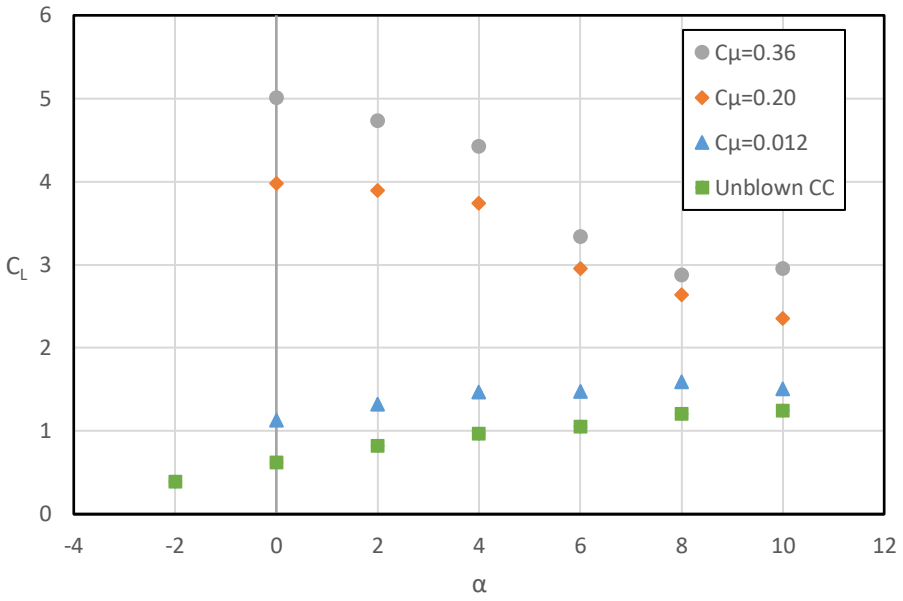

Figure 38. CL vs α for momentum coefficients in the boundary layer control region (0.012) and the super circulation region (0.20 and .036).

This change in stagnation point location is also impacted by the wall effect from the wind tunnel domain. It will be discussed in section 5.1.3 specifically how the wind tunnel domain impacts the stagnation point location.

Circulation control has a significant impact on the chord-wise lift distribution on the airfoil. Based on the surface pressure coefficient plot in Figure 39 the chord-wise lift distribution is more evenly distributed along the chord compared to the unblown case. This is due to the circulation control blowing at the trailing edge creating a large low pressure zone. This has a significant impact on the aerodynamic center of the airfoil. On a typical unblown airfoil the aerodynamic center is close to c/4, whereas the circulation control airfoil when operating in the blowing configuration has the aerodynamic center near c/2.

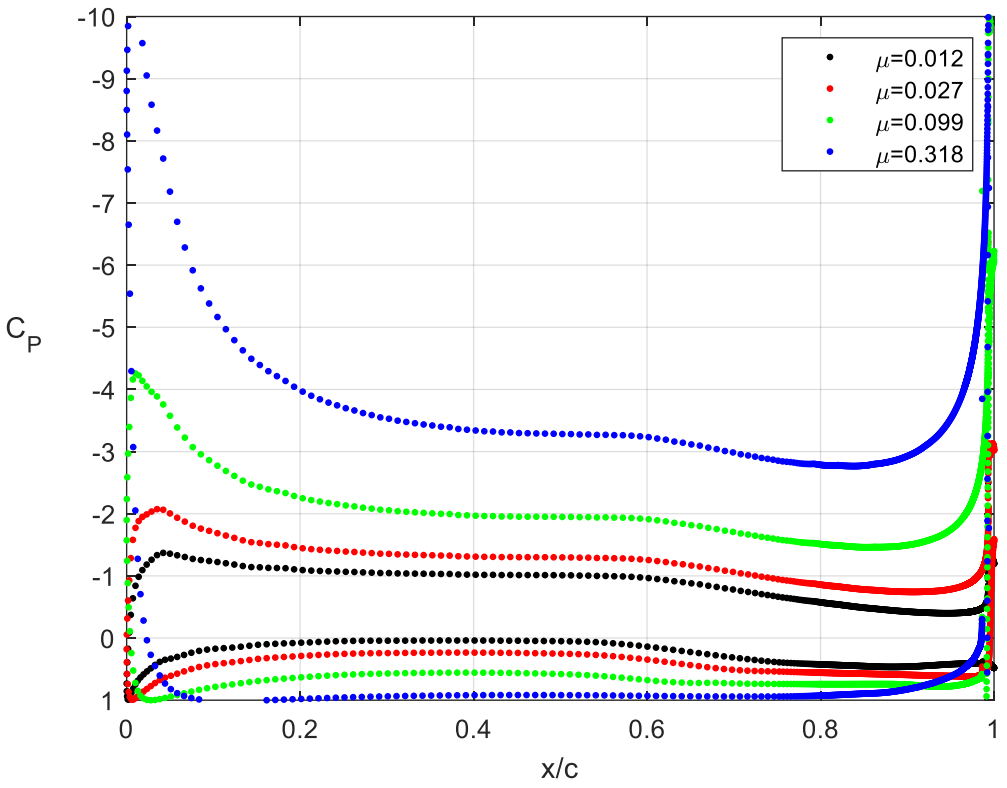

Figure 39. Pressure coefficient over airfoil surface for increasing momentum coefficients

The chord-wise lift distribution shifting aft creates a significant increase in nose down pitching moment which is shown in Figure 40. This is consistent with other circulation control wing designs. [12] $C_{M\alpha}$ varies linearly with C_L at α=0 where momentum coefficient is swept from 0 to 0.35.

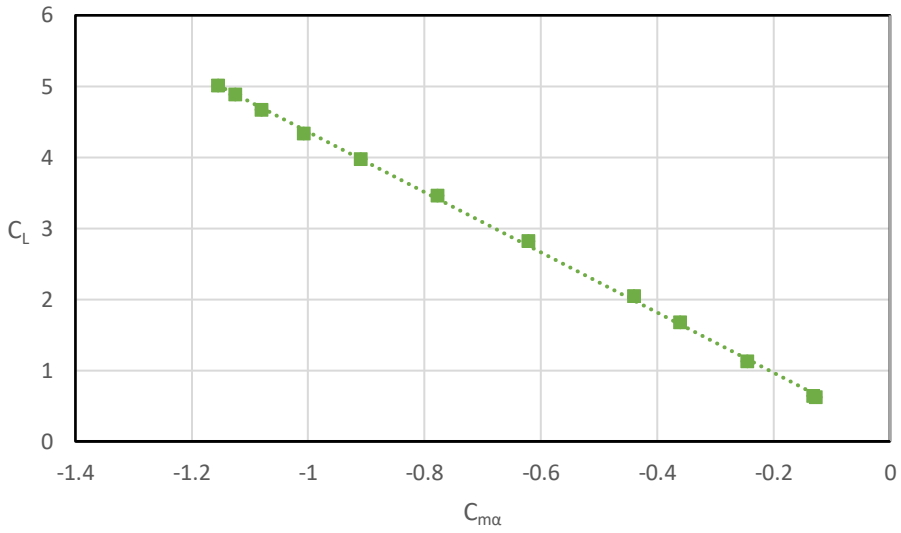

Figure 40. Pitching moment about c/4 vs lift coefficient for the CPCC airfoil at α=0. The momentum coefficient was swept from 0 to 0.35.

The magnitude of the tunnel wall pressure coefficient profile is shown in Figure 41 for varying momentum coefficients at 0 AoA. The pressure distribution on the tunnel wall is similar to typical high lift configurations being tested in a wind tunnel. [2] This also demonstrates that the circulation control jet does not directly impinge on the tunnel walls, but the increase in circulation around the wing creates a large pressure signature. Methods typically used to correct for high lift device wall effects can be implemented here.

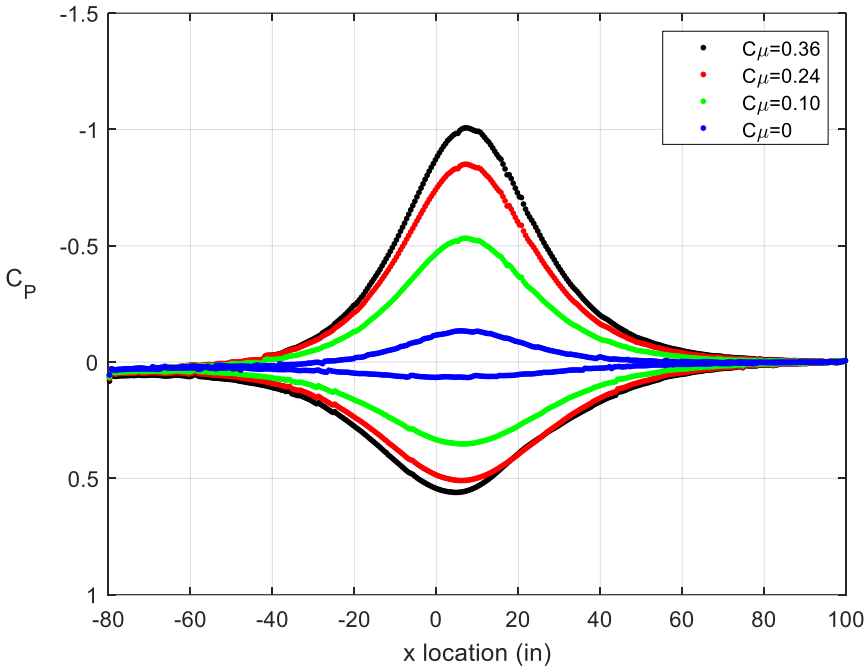

Figure 41. Pressure coefficient along the tunnel walls at different momentum coefficient values. AoA=0. The negative pressure values are the upper wall and the positive pressure values are the lower wall.

During experimental testing it is recommended to utilize static pressure ports along the tunnel walls to quantify this impact. Since these results are from 2D simulations, it would be beneficial to obtain the full 3D data experimentally. This would provide experimental data that will allow better estimations of wall impact on the flow. Due to the spanwise variance in the circulation, it may be useful to have multiple streamwise rows of static pressure ports corresponding to the blown and unblown portions.

The flow in the jet became choked around $C_\mu = 0.15$, meaning it reached sonic conditions at the outlet. The subsequent supersonic expansion downstream of the jet exit introduces difficulty in directly measuring the jet exit velocity profile for a few reasons. The jet velocity, U_{jet}, that is used to calculate momentum coefficient should be the average of the fully expanded jet velocity, which occurs at different physical locations depending on the internal plenum pressure once the sonic condition is reached. This phenomenon can be seen in Figure 42. This implies direct measurement of the jet velocity with a hot wire probe is not valid past the choked condition.

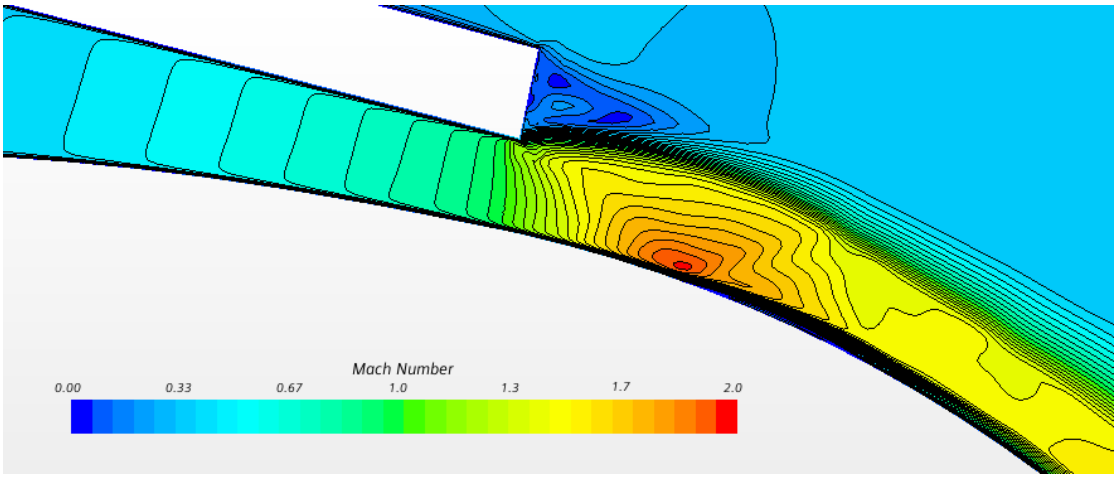

Figure 42. Mach scene with contour lines of the upper jet exit at C_μ=0.24 showing the choked flow and subsequent supersonic expansion. The slot height is 0.015".

Jet Mach number profiles are shown in Figure 43 for increasing momentum coefficients. Once the sonic condition is reached, the Mach profile remains relatively constant due to the choked flow. There is a small amount of supersonic expansion that occurs on the jet exit plane, however, this does not capture the full expansion of the jet. Capturing any supersonic flow in the choked nozzle is not expected, so this is likely due to an error in the simulation capturing the expansion around the sharp upper corner of the slot

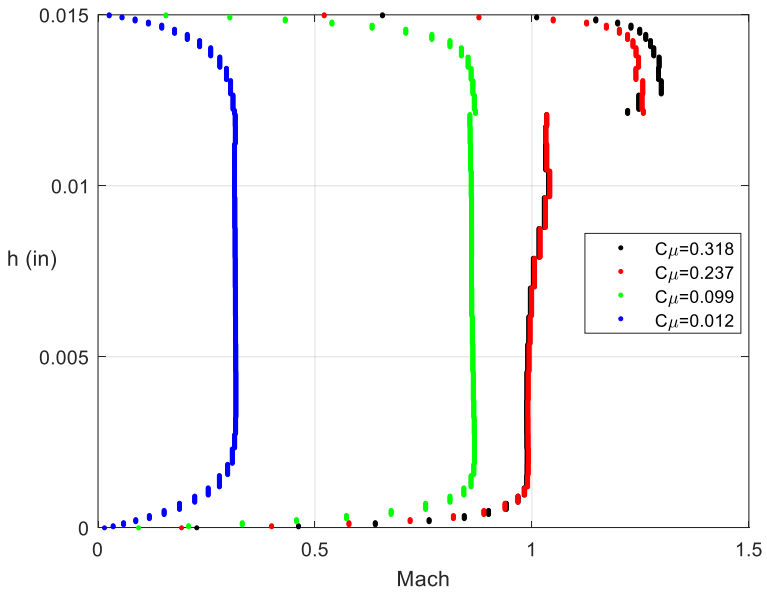

Figure 43. Mach number profiles for the upper jet exit slot at varying momentum coefficients with the line probe coincident with the slot exit plane. Note there is supersonic flow at the higher momentum coefficients

When sonic conditions are reached at the nozzle, this impacts how the jet velocity can be measured both in CFD and experimentally. As seen in Figure 44, using a line probe at the jet exit plane matches with the isentropic expansion equation well, up until the choke point. It may be valuable to try and experimentally measure the jet exit velocity with a hot wire probe to experimentally validate the isentropic expansion equation. However, experimental error due to the small slot height may not allow enough accuracy for this to be a worthwhile endeavor. Based on this it is recommended that the isentropic expansion equation is used to determine the jet velocity when doing experimental testing.

It should also be noted the high plenum pressures reached at the upper end of the tested range. At standard atmospheric freestream pressure, the internal plenum pressure exceeded 66psi. This along with the supersonic flow would create safety concerns, air supply concerns, and manufacturability concerns. Based on this, it is recommended for experimental testing that the choke point is not exceeded, or a plenum pressure ratio of ~2.

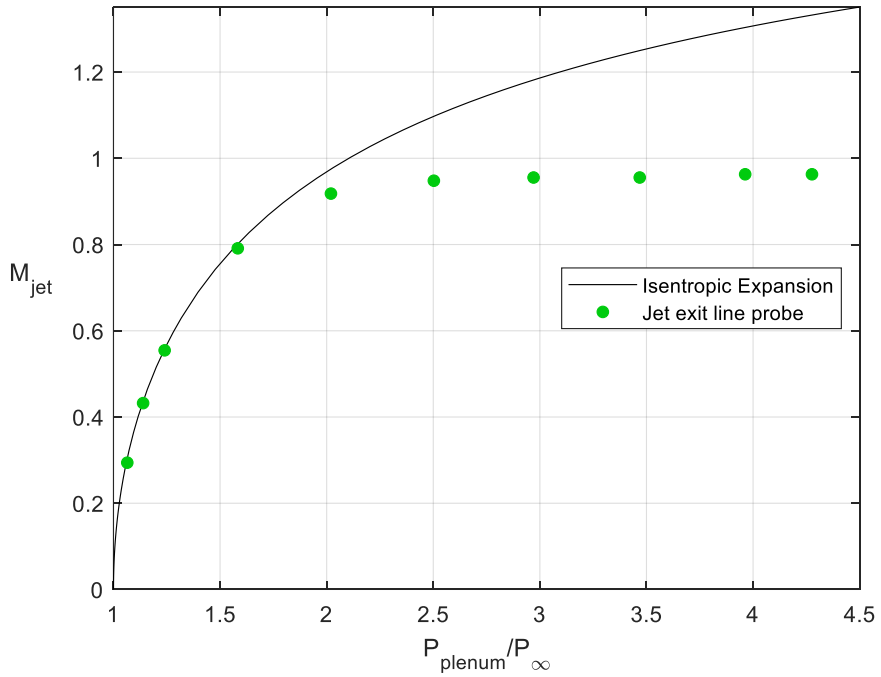

Figure 44. Jet Mach number versus nozzle pressure ratio for Isentropic expansion and measuring with a line probe at the jet exit

Measuring the separation location of the Coanda jet is an important parameter to determine experimentally, especially for future CFD validation efforts. As seen in Figure 45 the jet separation location can be experimentally determined by implementing static pressure ports on the Coanda surface. When the pressure coefficient equals 0, that indicates the jet has separated from the Coanda surface. With no blowing active, all of the flow behind the Coanda surface is separated. At $C_\mu = 0.012$, which is in the boundary layer control region, the jet flow separated from the surface at θ=115°. At $C_\mu = 0.026$, which is in the transition between boundary layer control and super circulation, the separation angle is θ=172°, demonstrating the flow remained attached roughly over the complete Coanda surface. This highlights another key aspect of circulation control flow: super circulation occurs when the flow remains fully attached around the Coanda surface.

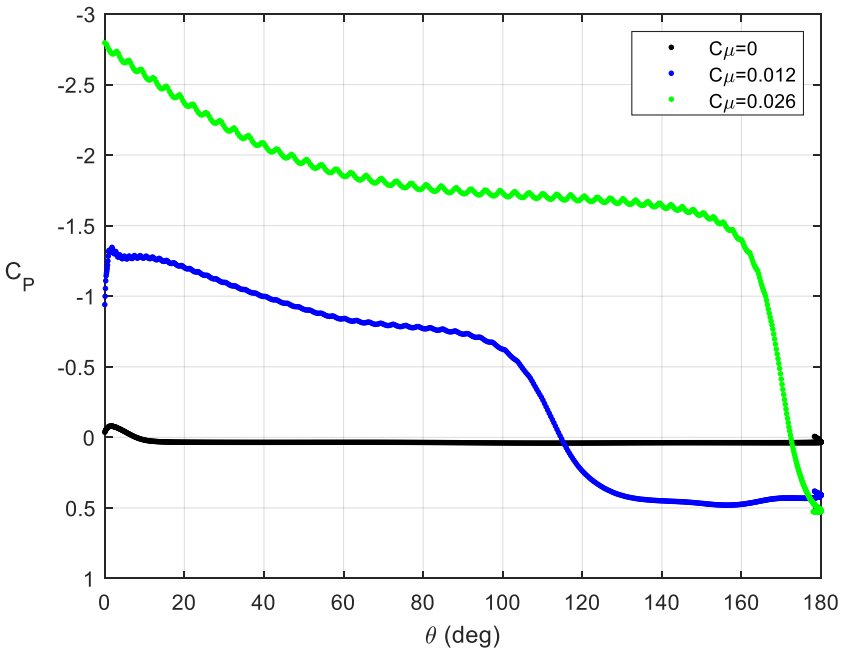

Figure 45. Pressure coefficient on the Coanda surface at different momentum coefficients.

In summary, the high lift configuration was shown to produce sectional lift coefficients up to 5, which could be further increased with increasing momentum coefficient. The high lift configuration produces a large nose down pitching moment compared to unblown airfoils. Two distinct regions, boundary layer control and super circulation control, are clearly defined in the lift

slope. The wind tunnel wall pressure distribution is similar to other high lift devices. The jet slot velocity profile became choked at $C_\mu = 0.15$, which demonstrates the need to calculate U_{jet} using the isentropic expansion equation.

5.1.3 Cruise Configuration

The cruise configuration for the wing utilizes dual blowing. Both the upper and lower blowing slots are active at independent momentum coefficients. A “pneumatic trailing edge” is effectively created as can be seen in Figure 46. The largest efficiency gain comes from operating the upper slot in the boundary layer control region. There are large drag penalties involved with higher momentum coefficients. There is a tradeoff using the jet flow to reduce cruise drag with the increased mass flow rate requirement.

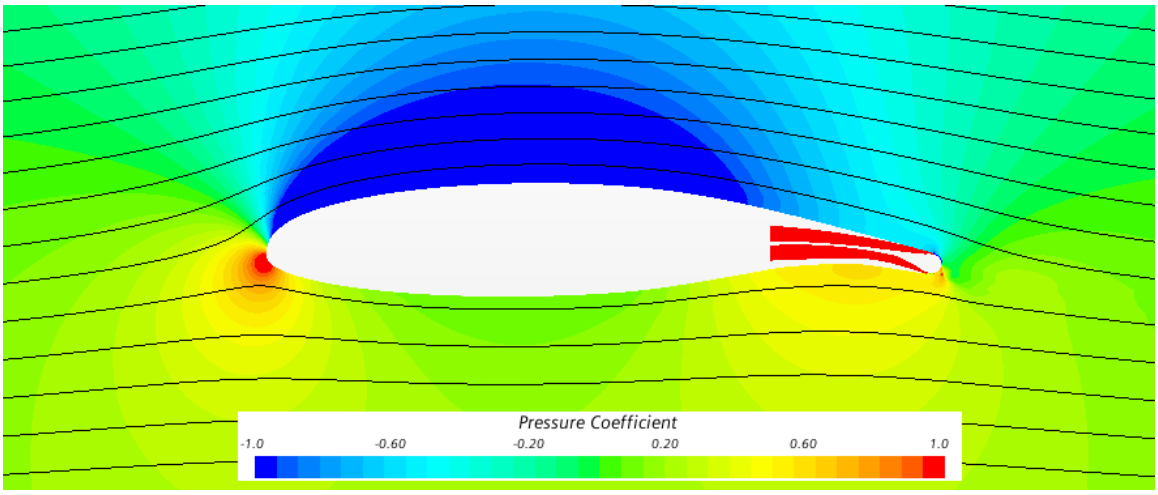

Figure 46. Streamlines are shown on a pressure coefficient scene with dual blowing. The upper slot is set to C_μ=0.012 and the lower slot is set to C_μ=0.003.

The detail view of the trailing edge at this condition can be seen in Figure 47. The upper slot has a momentum coefficient in the boundary layer control region. This helps reduce flow separation on the top surface of the wing and increases lift. The bottom jet for this case is set to half the mass flow rate of the upper jet, corresponding to a momentum coefficient ratio of 1:4. This is also in the boundary layer control region and the jet helps reduce the low pressure zone that would otherwise form on the lower portion of the trailing edge. It should be noted that an exhaustive set of upper and lower blowing rates were not tested here. It is encouraged for future work to determine the specific blowing ratios that optimize cruise performance.

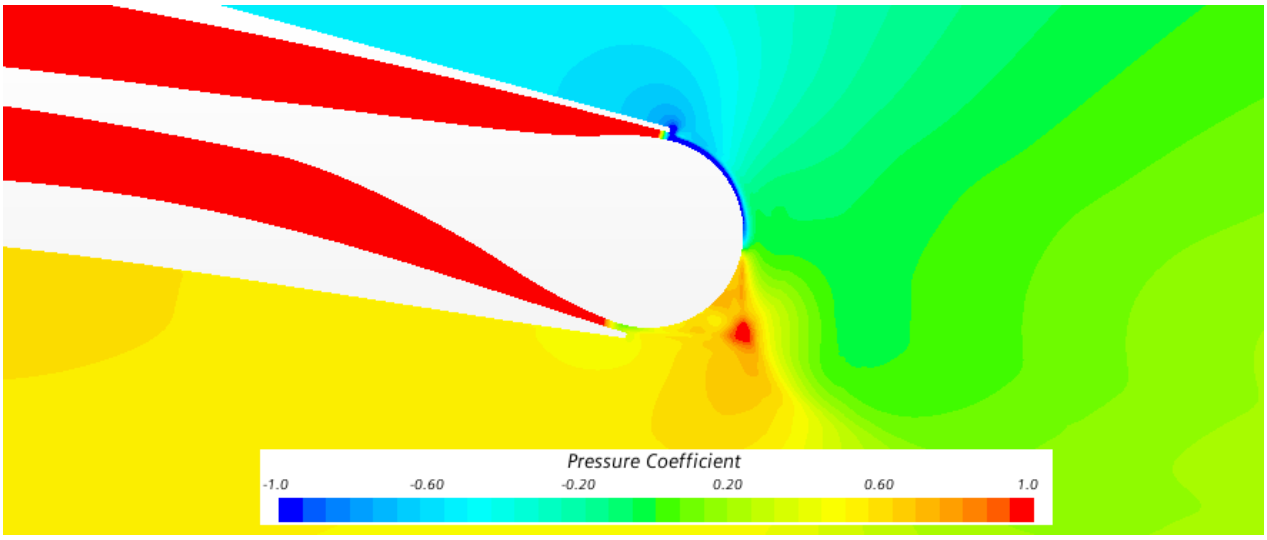

Figure 47. Detail view of the trailing edge with dual blowing. The “pneumatic trailing edge” can be seen with the rear stagnation point slightly aft of the wing surface. The upper slot is set to C_μ=0.012 and the lower slot is set to C_μ=0.003.

When correcting for the reaction thrust from the jets, the max L/D_{EQ} reached was 62.4 at a lift coefficient of 1.18. Using a linear interpolation from the experimental data of the unmodified LS(1)-0417 GA(W)-1 airfoil, the L/D at a lift coefficient of 1.18 was 61.3. This demonstrates the dual blowing configuration at specific conditions can match or exceed efficiencies of conventional sharp trailing edge airfoils. The minimum equivalent drag coefficient, $C_{D\ EQ}$, is dominated by the correction for the reaction jet portion of the equation even at the low C_μ shown. This is highlighted in that the C_μ term in the $C_{D\ EQ}$ equation is 80% of the equivalent drag for this specific momentum coefficient ratio.

During experimental testing it is recommended to use a wake rake, the load cell, and surface pressure measurements to fully quantify the drag produced. The load cell will measure the total forces and moments seen by the wing. However, this also includes any thrust produced by the jet blowing. It is desirable to isolate the thrust due to blowing from the induced drag on the wing. Using a wake rake downstream of the wing model can be used to determine the total pressure loss. When this data is used in conjunction with the energy added through circulation control a better idea of the span-wise drag distribution can be created. Surface pressure taps will provide a method to isolate just the pressure drag. These surface pressure taps are more important for determining sectional lift, but will also be useful for this case.

5.1.4 Freestream Comparison

The 2D wind tunnel model was compared to a 2D freestream model, where there were no bounding walls near the wing. This will help develop correction factors for wind tunnel testing to compensate for the experimental environment. The freestream model domain was sized so the upper and lower walls had no impact on the flow field, effectively simulating free air. A plot of lift coefficient versus momentum coefficient can be seen in Figure 48.

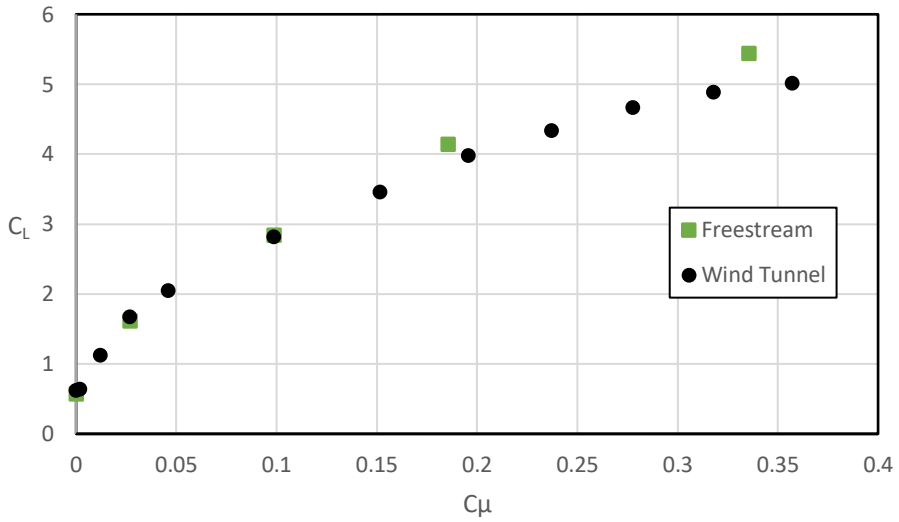

Figure 48. Lift coefficient vs momentum coefficient for the freestream domain and the wind tunnel domain.

The offset between the freestream domain and wind tunnel domain C_L was approximately 8% at the max C_μ. Agreement at lower momentum coefficients was increased substantially, with only 0.5% variance up to $C_\mu = 0.1$. The variance seems well behaved where it is increasing consistently as momentum coefficient is increasing. This implies that wind tunnel results can be reliably extrapolated to free air results. It should be noted that this is only valid for the 2D case and additional corrections will need to be applied to the 3D case because the 2D case does not simulate any of the juncture vortices that are prevalent in the 3D case.

Examining the location of the leading edge stagnation point was another method of quantifying the impact of the wind tunnel domain as seen in Figure 49. The freestream domain stagnation point is located at 0.16 x/c and the wind tunnel domain stagnation point is located at

0.13 x/c at a $C_\mu = 0.36$. At lower momentum coefficients where the lift coefficients align well, the stagnation points locations are the same.

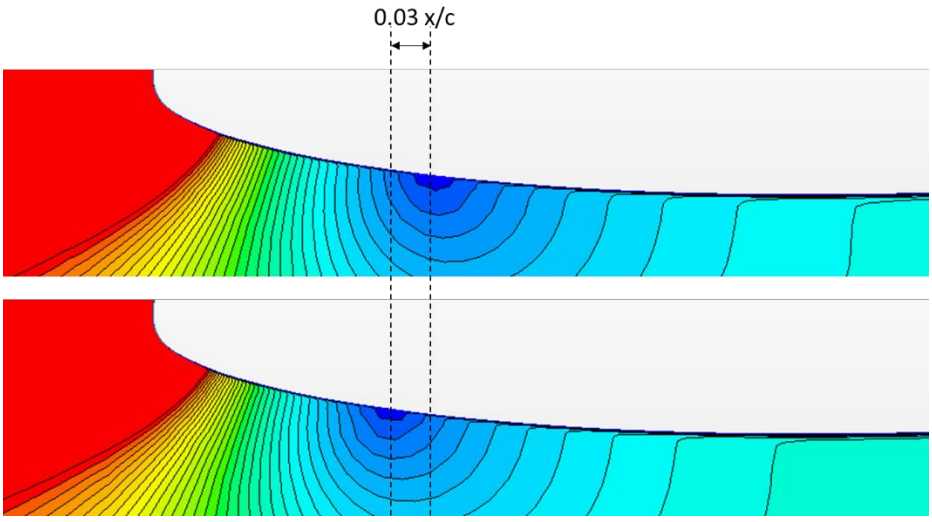

Figure 49. Mach contour scene showing the leading edge stagnation point (dark blue) at C_μ=0.36 for the freestream (top) and wind tunnel (bottom) domain.

Streamline turning was also impacted by the wind tunnel domain compared to the freestream domain. This impact is most evident at high momentum coefficients as seen in Figure 50 which shows the streamlines at $C_\mu = 0.36$. The wind tunnel walls force parallel flow at the wall boundaries, which eliminates some of the overall streamline turning that is present in freestream conditions. This is one of the factors that caused the wind tunnel domain to underpredict lift at higher momentum coefficients.

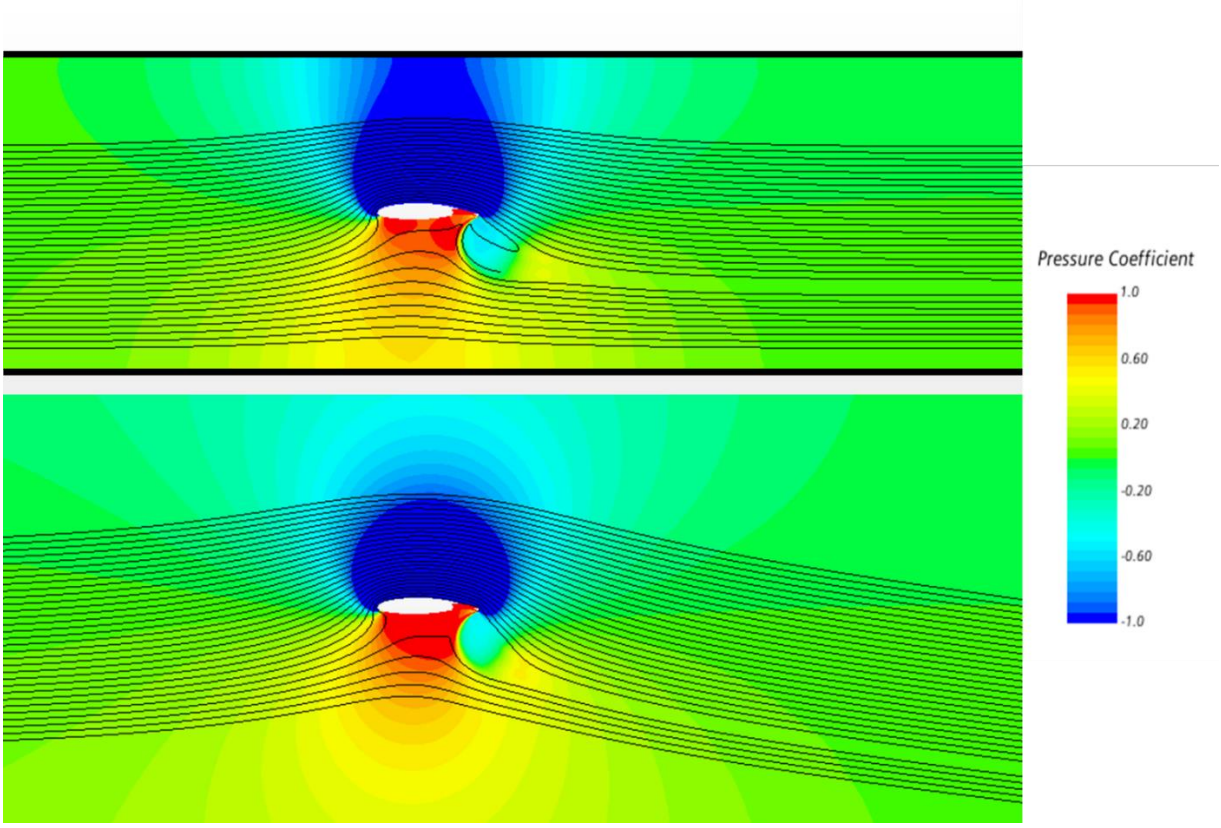

Figure 50. Wind tunnel domain (top) and freestream domain (bottom) with streamlines demonstrating flow turning.

5.2 3D CFD Results

Two 3D test cases were simulated, no blowing and blowing, to demonstrate the impact of finite span blowing and get a baseline for the wing in the tunnel. Likely due to the limitations on mesh size, the solution did not converge to a degree to provide high confidence in the results; the residuals were on the order of 10^{-3}, which is considered poorly converged. This was after 35,000 iterations and the lift coefficient became asymptotic. Quantitative results were not taken from this, however qualitative aspects of the flow still give some insight into how the wing would likely perform in a wind tunnel domain.

The streamlines show the vortices forming at the juncture between the blown and unblown portion both inboard and outboard which can be seen in Figure 51. This is due to the sharp change in lift produced between the blown and unblown portions. The strength of these

vortices depends on the momentum coefficient. Based on the 2D simulation, the sectional lift coefficient at $C_\mu = 0.055$ was approximately 2, while the unblown wing had a sectional lift coefficient of 0.62.

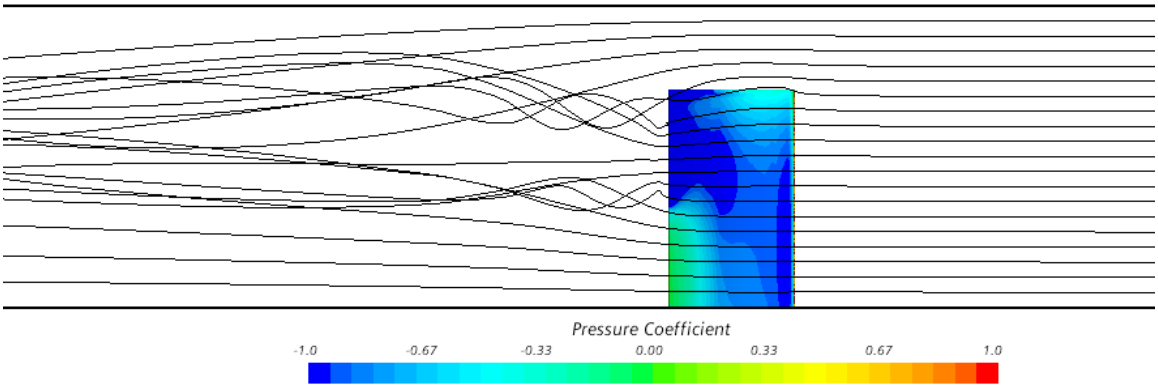

Figure 51. 3D simulation with streamlines and surface pressure coefficient at C_μ=0.055

Based on the size of these vortices compared to the blowing slot span, the overall efficiency of the circulation control is greatly reduced. Quantifying this impact will be an important aspect of wind tunnel testing. Measuring the extent and intensity of these vortices would be best completed using a wake rake including an array of 7-hole probes that can be traversed along the span. The 7-hole probes in this case are better suited than typical pitot probes used in a wake rake due to the high angularity of the flow.

Chapter 6

CONCLUSIONS AND FUTURE WORK

6.1 Testing recommendations

Consistent measurement techniques for the jet slot velocity are one of the most important aspects for experimental investigation into circulation control. To determine the jet velocity, the isentropic expansion as shown in equation 1.15 should be used. When comparing this calculation to the line probe at the jet exit, the isentropic expansion characterizes the jet velocity well. Directly measuring the jet velocity at the exit only works before the choked condition is reached. The required experimental measurements to use the isentropic expansion equation are plenum pressure, plenum temperature, and freestream pressure. This would require a pitot probe in the plenum to measure total pressure, and a thermocouple in the plenum to measure the temperature. It is recommended to have 3 spanwise internal total pressure probes to ensure the internal plenum flow is consistent. The wind tunnel freestream total pressure is measured by instrumentation built into the tunnel.

Slot height is another key parameter involved in calculating the momentum coefficient. It is recommended that sufficient structure is added to ensure the slot height remains consistent along the span of the wing as well as when the momentum coefficient changes. The internal plenum can reach pressures up to 66 psi at the momentum coefficients that were investigated here. These high plenum pressures are due to the choked condition and are not realistic to test in the CPLSWT. It is recommended that the experimental testing does not exceed the choked condition. The plenum pressure prior to the choked condition is 15 PSI which can be safely provided via the shop air line. Measurements of the slot height should be taken at both loaded and unloaded conditions to verify the change that occurs from pressurizing the plenum.

In order to measure the total forces and moments on the wing, it is desirable to use a 5 or 6 axis load cell that can measure lift force, drag force, pitching moment, and roll moment. This will be mounted at the root of the wing isolated from the air supply lines. The total force and moment

measurements can be used in conjunction with the sectional measurements and wake rake measurements.

Quantifying the impact the slot-end vortices have on the sectional lift coefficient requires the use of surface pressure taps on the wing surface at multiple span-wise locations. Desired positions would be centerline of the blowing slot, the juncture of the blowing and unblown portion, and centerline of the unblown portion. This will allow an experimental investigation into how the transition between blown and unblown sections impact blowing efficiency. There should also be surface pressure taps on the Coanda surface in-line with the wing surface pressure taps. In addition to determining sectional lift coefficients, this can be used to determine the Coanda jet separation angle.

To better quantify the drag and the strength of the juncture vortices a wake rake comprised of 5-hole probes is desired. The wake rake would likely be a linear rake that in addition to capturing the total pressure loss could determine the vortex strength. The CPLSWT has the capability to traverse the rake along the span of the wing to fully capture the 3D total pressure loss behind the wing.

A final recommendation is to use a particle image velocimetry (PIV) system to characterize the full flow field. At the time of writing, Cal Poly is in the process of getting their PIV system working for the CPLSWT. This would be able to provide valuable data of the complete velocity field in the tunnel and allow more complete CFD validation efforts.

6.2 Conclusions

The numerical analysis performed for this thesis provided valuable insight into how the CPCC wing would behave in a wind tunnel environment. There was data collected for both wind tunnel and freestream domains for 2D simulations. The 3D simulations have room for improvement.

The requirements set for the airfoil performance were all met. The airfoil was simulated up to the point of a sectional lift coefficient of 5 at $C_\mu = 0.36$, which can provide STOL capabilities to an aircraft this is applied to. However, operating at these conditions is not realistic in the

CPLSWT environment. The recommended max C_μ for experimental investigation is 0.15 which is just prior to the choked condition. It was noted that the airfoil began to stall at low angles of attack in the super circulation region ($C_\mu > 0.05$) while the boundary layer control region ($C_\mu < 0.05$) did not have a significant impact on stall angle.

The dual blowing capability was shown to improve the L/D_{EQ} of the airfoil to a point where it was equivalent to the unmodified airfoil with a sharp trailing edge at a lift coefficient of 1.2. The minimum equivalent drag coefficient for the CPCC airfoil was still 40% higher than the drag coefficient of the unmodified airfoil.

The CPCC wing was intended to provide a test bed for circulation control technology, rather than perform as an optimally designed wing. The purpose was to be able to isolate the effect of circulation control blowing and better quantify the 3D effects that occur. It was shown through numerical simulation that the juncture vortices will have a significant impact on the efficiency of the wing, and this is an important feature to quantify experimentally.

6.3 Future work

The next step is to build an experimental model based on the design created herein. The goal of this thesis was to provide recommendations on ways to ensure the testing provides useful data. The actual construction of the test article will be a complex endeavor, however based on the analysis and recommendations from previous research compiled here this task should become much more focused.

One area that would benefit from further investigation is full 3D CFD simulations of a circulation control wing where improved hardware is available. Mesh sizes up to 50-100 million cells may be necessary to fully capture the jet flow and the induced shear layer in the wake region. Since these are low speed and high speed flows with significant mixing going on, smaller time steps must be taken to converge to a solution, which extends computational time. It is desirable to get reliable data from the wind tunnel testing campaign which can be used for 3D CFD validation efforts.

An experimental model will allow for more complete sweep of blowing coefficients. Each 3D simulation can take on the order of 7 days to converge to a solution depending on the specific hardware available and mesh size, whereas a full sweep of blowing coefficients can be completed experimentally in one day. This would allow for further optimization of the momentum coefficient ratio between the blowing slots to minimize drag.

Mass flow requirements for the jet are the main driver of efficiency in terms of lift coefficient per momentum coefficient. It is recommended that other ways to reduce mass flow rate, while maintaining performance characteristics, be investigated. There have been previous investigations into pulsed blowing that have shown to be beneficial.

WORKS CITED

[1] Anderson, J. D. (2011). *Fundamentals of Aerodynamics.* New York: McGraw-Hill.

[2] Barlow, J. B., William H. Rae, J., & Pope, A. (1999). *Low-Speed Wind Tunnel Testing.* John Wiley & Sons.

[3] Ehrmann, R. S. (2010). *Development of Measurement Methods for Application to a Wind Tunnel Test of an Advanced Transport Model.* San Luis Obispo: California Polytechnic State University.

[4] Englar, R. J. (2000). *Circulation Control Pnuematic Aerodynamics: Blown Force and Moment Augmentation and Modification; Past, Present, and Future.* AIAA.

[5] Engler, R. J. (1975). *Experimental Investigation of the High Velocity Coanda Wall Jet Applied to Bluff Trailing Edge Circulation Control Airfoils.* Naval Ship Research and Development Center.

[6] Hu, J., Wang, Z., Zhao, W., Sun, S., Sun, C., & Guo, C. (2020). Numerical Simulation on Vortex Shedding from a Hydrofoil in Steady Flow. *Journal of Marine Science and Engineering*.

[7] Jones, G. S. (2005). *Pneumatic Flap Performance for a 2D Circulation Control Airfoil, Steady and Pulsed.* NASA.

[8] Jones, G. S., Viken, S. A., Washburn, A., Jenkins, L. N., & Cagle, C. (2002). *An Active Flow Circulation Controlled Flap Concept for General Aviation Aircraft Applications.* AIAA.

[9] Jones, G., Lin, J., Allan, B., Milholen, W., Rumsey, C., & Swanson, R. (2008). *Overview of CFD Validation Experiments for Circulation Control Applications at NASA.* NASA.

[10] Lichtwardt, J., Paciano, E., Jameson, D. T., Fong, R., & Marshall, D. D. (2012). *Advanced Model for Extreme Lift and Improved Aeroacoustics (AMELIA).* NASA.

[11] M., Y. E., Beck, N., Kumar, P., Semaan, R., & Radespiel, R. (2018). *Challenges in the experimental Quantification of the Momentum Coefficient of Circulation Controlled Wings.* Braunschweig: Institute of Fluid Mechanics, TU Braunschweig.

[12] Marshall, D. D., & Jameson, K. K. (2010). *Overview of Recent Circulation Control Modeling Activities at Cal Poly.* AIAA.

[13] McGhee, R. J., & Beasley, W. D. (1981). *Wind-Tunnel Results for a Modified 17-Percent-Thick Low-Speed Airfoil Section.* Hampton: NASA.

[14] Nichols, J. H., & Harris, M. J. (1988). *Fixed Wing CCW Aerodynamics With and Without Supplementary Thrust Deflection.* Department of the Navy.

[15] Pharo, J., & Marshall, D. D. (2011). *Improved Meshing Technique for the Engine Exhaust of an Over-the-Wing Engine and Circulation Control Wing Configuration.* AIAA.

[16] Roache, P. J. (1997). Quantification of uncertainty in computational fluid dynamics. *Annual Review of Fluid Mechanics vol. 29*, 123-160.

[17] San Diego Air and Space Museum Archive. (1977). *Grumman A-6A 151568 Circulation Control Wing prototype 1977.* Retrieved from https://www.flickr.com/photos/sdasmarchives/17134060572/

[18] Siemens. (n.d.). Star CCM+ User Database.

[19] Smith, A. (1975). *High-Lift Aerodynamics.* AIAA.